Dynein light chain regulates axonal trafficking and synaptic levels of Bassoon

Anna Fejtova,[1] Daria Davydova,[1] Ferdinand Bischof,[1] Vesna Lazarevic,[1] Wilko D. Altrock,[1] Stefano Romorini,[1] Cornelia Schöne,[1] Werner Zuschratter,[2] Michael R. Kreutz,[3] Craig C. Garner,[4] Noam E. Ziv,[5,6,7] and Eckart D. Gundelfinger[1]

[1]Department of Neurochemistry and Molecular Biology, [2]Special Laboratory for Electron and Laserscannning Microscopy, and [3]Project Group Neuroplasticity, Leibniz Institute for Neurobiology, D-39118 Magdeburg, Germany
[4]Nancy Pritzker Laboratory, Department of Psychiatry and Behavioral Science, Stanford University School of Medicine, Stanford, CA 94305
[5]The Rappaport Family Institute for Research in Medical Sciences, [6]Department of Physiology and Biophysics, and [7]The Lorry Lokey Interdisciplinary Center for Life Sciences and Engineering, Technion–Israel Institute of Technology, Haifa 32000, Israel

Bassoon and the related protein Piccolo are core components of the presynaptic cytomatrix at the active zone of neurotransmitter release. They are transported on Golgi-derived membranous organelles, called Piccolo-Bassoon transport vesicles (PTVs), from the neuronal soma to distal axonal locations, where they participate in assembling new synapses. Despite their net anterograde transport, PTVs move in both directions within the axon. How PTVs are linked to retrograde motors and the functional significance of their bidirectional transport are unclear. In this study, we report the direct interaction of Bassoon with dynein light chains (DLCs) DLC1 and DLC2, which potentially link PTVs to dynein and myosin V motor complexes. We demonstrate that Bassoon functions as a cargo adapter for retrograde transport and that disruption of the Bassoon–DLC interactions leads to impaired trafficking of Bassoon in neurons and affects the distribution of Bassoon and Piccolo among synapses. These findings reveal a novel function for Bassoon in trafficking and synaptic delivery of active zone material.

Introduction

In neurons, the transport of membranous organelles along axons is based on molecular motors that propel organelles along microtubules, which, in axons, are oriented uniformly, with their plus ends pointing toward the growing tips (Burton and Paige, 1981). Anterograde transport is driven by members of the kinesin family of molecular motors, whereas retrograde transport relies mainly on the cytoplasmic dynein 1 motor complex (Vale, 2003). The role of anterograde transport in trafficking of axonal proteins is well documented, and molecular motors carrying axonal cargoes were identified (Hirokawa and Takemura, 2005). Two classes of vesicular cargoes were studied in the context of presynaptic assembly in neurons; synaptic vesicle (SV) precursors transported by kinesin-3 heavy chain KIF1A (Okada et al., 1995) probably linked via the cargo adapter liprin-α (Shin et al., 2003; Miller et al., 2005), and Piccolo-Bassoon transport vesicles (PTVs) linked via the syntaxin1–syntabulin adapter complex to KIF5B, which is the heavy chain of conventional kinesin-1 (Cai et al., 2007). Imaging of most anterogradely transported axonal cargoes reveals that they move bidirectionally (Schroer et al., 1985; Shapira et al., 2003; Miller et al., 2005), suggesting that most cargoes are able to associate with both anterograde and retrograde motors. However, little attention has been paid to the understanding of the molecular mechanisms and physiological meaning of retrograde transport of material predestined for delivery to distal axonal locations.

Bassoon and Piccolo (also named Aczonin) are highly homologous core components of CAZ (cytomatrix at the active zone; tom Dieck et al., 1998; Wang et al., 1999; Fenster et al., 2000). They are large scaffold proteins believed to functionally and spatially organize presynaptic neurotransmitter release (Fejtova and Gundelfinger, 2006; Leal-Ortiz et al., 2008). After synthesis, they associate with Golgi-derived membranous

Correspondence to Anna Fejtova: afejtova@ifn-magdeburg.de; or Eckart D. Gundelfinger: gundelfi@ifn-magdeburg.de

Abbreviations used in this paper: DBM, DLC-binding mutant; DHC, dynein heavy chain; DIV, day in vitro; DLC, dynein light chain; ICC, immunocytochemistry; mRFP, monomeric RFP, MTOC, microtubule-organizing center; OC, overlap coefficient; PTV, Piccolo-Bassoon transport vesicle; SV, synaptic vesicle; WB, Western blot.

The Rockefeller University Press $30.00
J. Cell Biol. Vol. 185 No. 2 341–355
www.jcb.org/cgi/doi/10.1083/jcb.200807155

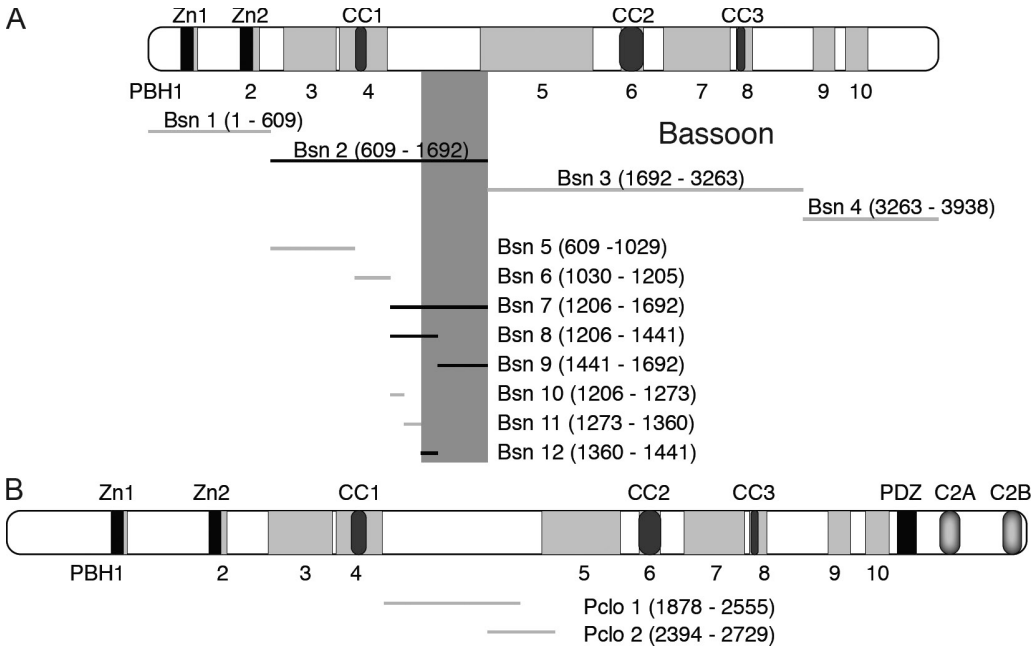

Figure 1. **Mapping of the DLC-binding region on Bassoon.** (A) Overview of Bassoon fragments tested for binding to DLC1 in yeast two-hybrid assays. The extension of positive Bsn clones is displayed in black, and nonbinding clones are indicated in gray. (B) The homologous region of Piccolo does not bind DLC. Amino acid residues encoded by individual subclones are given in parentheses. Zn1/2, zinc fingers; CC1–3, coiled-coil regions; PDZ, PSD-95/Dlg/zonula occludens-1 homology domain; C2A/B, C2 domains; PBH1–10, regions of the Piccolo-Bassoon homology domain (depicted as gray boxes).

organelles that are transported along axons to sites of nascent synaptic contacts (Zhai et al., 2001; Bresler et al., 2004; Dresbach et al., 2006; Tao-Cheng, 2007). It was shown that the accumulation of Bassoon and Piccolo at nascent synaptic junctions temporally correlates with activity-induced SV recycling and often precedes clustering of postsynaptic elements (Friedman et al., 2000; Zhai et al., 2000; Shapira et al., 2003). Thus, it was postulated that they might play an important role in the formation of presynaptic release sites early in synaptogenesis (Fejtova and Gundelfinger, 2006).

Dynein light chain (DLC) LC8 represents one of three dimeric light chains of the cytoplasmic dynein motor complex (Vallee et al., 2004; Pfister et al., 2005). In mammals, two DLC isoforms, DLC1 and DLC2, were reported to link cargoes to the dynein motor (Schnorrer et al., 2000; Navarro et al., 2004; Lee et al., 2006) to associate with the actin-dependent motor myosin V (Espindola et al., 2000), where it might also function as a cargo adapter (Puthalakath et al., 2001), and to have additional motor-independent cellular functions (Jaffrey and Snyder, 1996; Vadlamudi et al., 2004).

In this study, we describe an interaction of DLC1 and DLC2 with Bassoon and demonstrate that DLC-binding fragments of Bassoon function as cargo adapters for retrogradely moving organelles. Bassoon associates with the dynein motor complex in neurons, and disruption of Bassoon–DLC binding results in deficits in axonal trafficking of PTVs in living neurons. Our findings reveal a novel function of Bassoon (i.e., directly connecting PTVs to molecular motors), thus assuring their active transport toward nascent synapses. Moreover, they provide new insights on the importance of bidirectional transport for appropriate cargo trafficking during synapse formation.

Results

Bassoon can interact with DLC1 and DLC2

To identify novel proteins interacting with Bassoon, the cDNA fragment Bsn2 covering aa 609–1,692 of rat Bassoon (Fig. 1) was used as bait in a yeast two-hybrid screen. Seven independent positive clones carried the cDNA of DLC1. In subsequent experiments, the DLC-binding interface of Bassoon was narrowed down to fragment Bsn12 (aa 1,360–1,441) and Bsn9 (aa 1,441–1,692). Baits covering the other parts of Bassoon did not show any binding (Fig. 1 A). The binding region (fragment Bsn7), which is situated between two Piccolo-Bassoon homology domains, does not contain any predictable structural features. Moreover, an alignment of the amino acid sequence between PBH4 and PBH5 with the corresponding Piccolo region showed only 10% identity and 17.4% similarity. In line with this, overlapping constructs Pclo1 and Pclo2 covering the corresponding region of rat Piccolo (aa 1,878–2,729) did not interact with DLC1 in yeast, implying that the DLC1 interaction interface of Bassoon is not conserved in Piccolo (Fig. 1 B). DLC2 also interacted with fragments Bsn12 and Bsn9 but not with Pclo1 and Pclo2 in yeast.

To confirm the yeast two-hybrid analyses, an interaction of Bassoon's DLC-binding region with DLC1 and DLC2 was examined in corecruitment assays after heterologous expression in COS-7 cells. GFP-tagged DLC1 or DLC2 was targeted to the outer mitochondrial membrane by fusing it with the mito-targeting sequence of the rat mitochondrial protein TOM20. Staining of transfected cells with MitoTracker demonstrated mitochondrial targeting of Mito-EGFP-DLC1, Mito-EGFP-DLC2, and the control fusion protein Mito-EGFP (Fig. S1). Fragment Bsn7 fused to monomeric RFP (mRFP) exhibited a rather uniform distribution

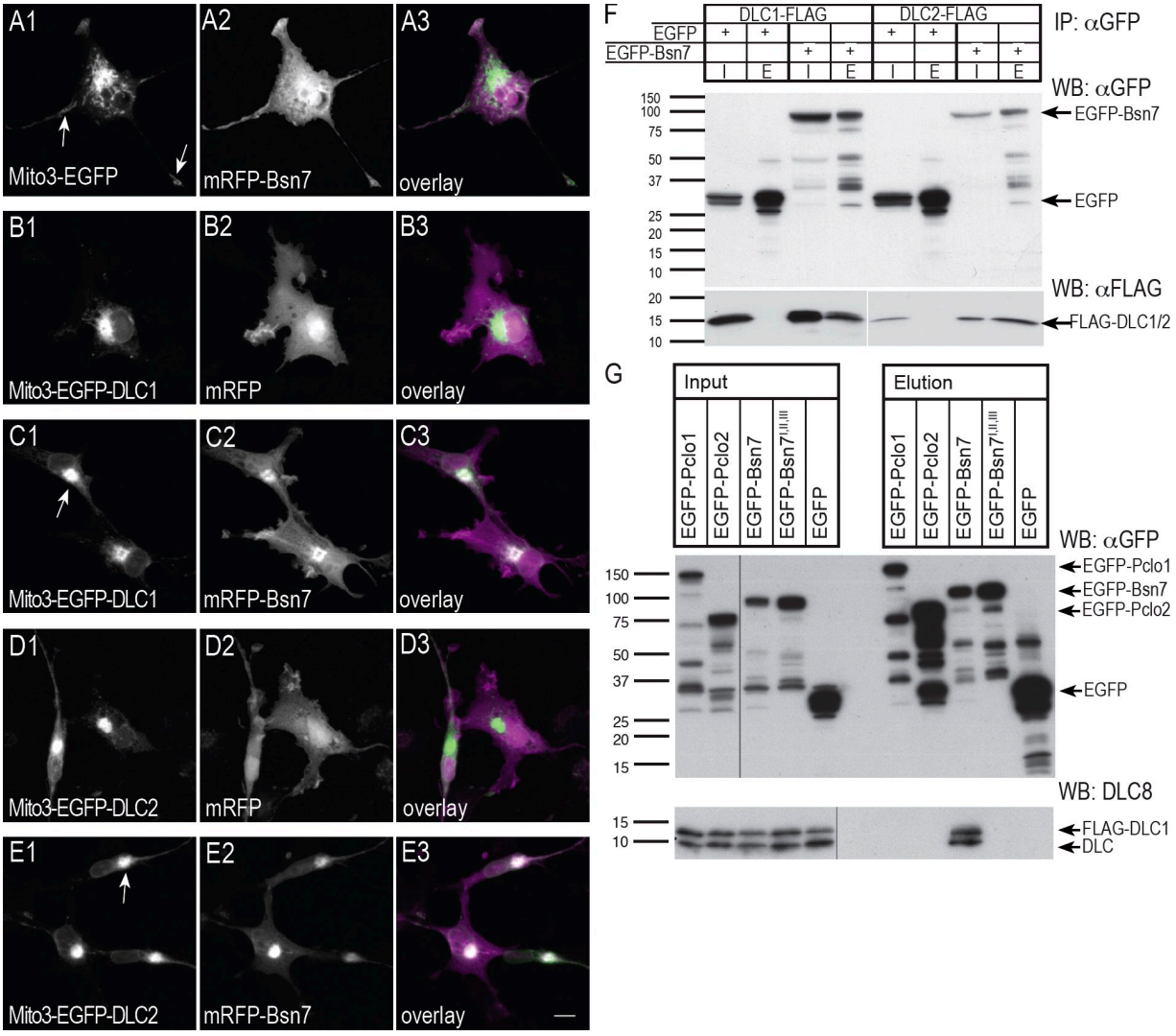

Figure 2. **Bassoon interacts with DLC1 and DLC2 in mammalian cells.** (A–E) Mito-targeting assays in COS-7 cells. Cells were fixed 18 h after transfection. Mito-targeted EGFP or EGFP-DLCs are localized at mitochondria (compare A1–E1 with Fig. S1). Bsn7 shows a uniform cytoplasmic distribution when coexpressed with Mito-EGFP control construct (A2) but is corecruited to mitochondria when mito-targeted DLC1 or DLC2 are coexpressed (C2 and E2). Targeting of DLC to mitochondria does not affect the localization of mRFP (B2 and D2). The arrows in A1 indicate the normally distributed localization of mitochondria in cell protrusions. In contrast, mitochondria are clustered near the cell centers when Mito-EGFP-DLC1 and Mito-EGFP-DLC2 are expressed (C1 and E1, arrows). (F and G) Coimmunoprecipitation of the Bassoon–DLC1/2 complexes from HEK293T cells. Lysates from transfected cells with EGFP-tagged Bsn7, Bsn7^{I,II,III}, Pclo1, or Pclo2 and Flag-tagged DLCs were incubated with anti-GFP antibodies coupled to magnetic beads. WBs of input material (I and Input lanes) and eluates (E and Elution lanes) detected with antibodies against GFP (top), anti-Flag (F, bottom), or with DLC8 antibody (G, bottom). All expressed EGFP-tagged proteins (I and Input lanes) were successfully immunoprecipitated (E and Elution lanes, arrows). (F) DLC1 and DLC2 were co-immunoprecipitated with EGFP-Bsn7 but not with EGFP. (G) Overexpressed DLC1 and endogenous DLC were precipitated with Bsn7 but not with the DBM Bsn7^{I,II,III}, Pclo1 and Pclo2 constructs, and EGFP. Black lines indicate that intervening lanes have been spliced out. (F and G) Molecular mass is indicated in kilodaltons. IP, immunoprecipitation. Bar, 10 µm.

in the cytoplasm when coexpressed with Mito-EGFP (Fig. 2, A2). In contrast, mRFP-Bsn7 was recruited to mitochondria when coexpressed with Mito-EGFP-DLC1 or Mito-EGFP-DLC2 (Fig. 2, C2 and E2). Recruitment of mRFP to mitochondria could not be detected when cotransfected with Mito-EGFP-DLC1 or Mito-EGFP-DLC2 (Fig. 2, B2 and D2).

Bassoon–DLC1 and –DLC2 complexes could also be isolated from heterologously expressing cells. To this end, Flag-tagged DLC1 or DLC2 were expressed together with EGFP-Bsn7 in HEK293T cells, and immunoprecipitation experiments were performed on cell lysates 48 h later using anti-GFP antibodies. Western blot (WB) analysis confirmed the successful coprecipitation of EGFP-Bsn7 with overexpressed DLC1 and DLC2 (Fig. 2 F) and with endogenous DLC (Fig. 2 G), demonstrating the existence of Bassoon–DLC complexes in living cells. In contrast, neither EGFP-Pclo1 nor EGFP-Pclo2 coprecipitated with recombinant DLC1 or endogenous DLC (Fig. 2 G). In control experiments, we were unable to coimmunoprecipitate DLC1 or DLC2 when coexpressed with EGFP. Collectively, binding assays in yeast and mammalian cells demonstrate that Bassoon can interact with both DLC1 and DLC2 via an interaction interface not conserved in Piccolo.

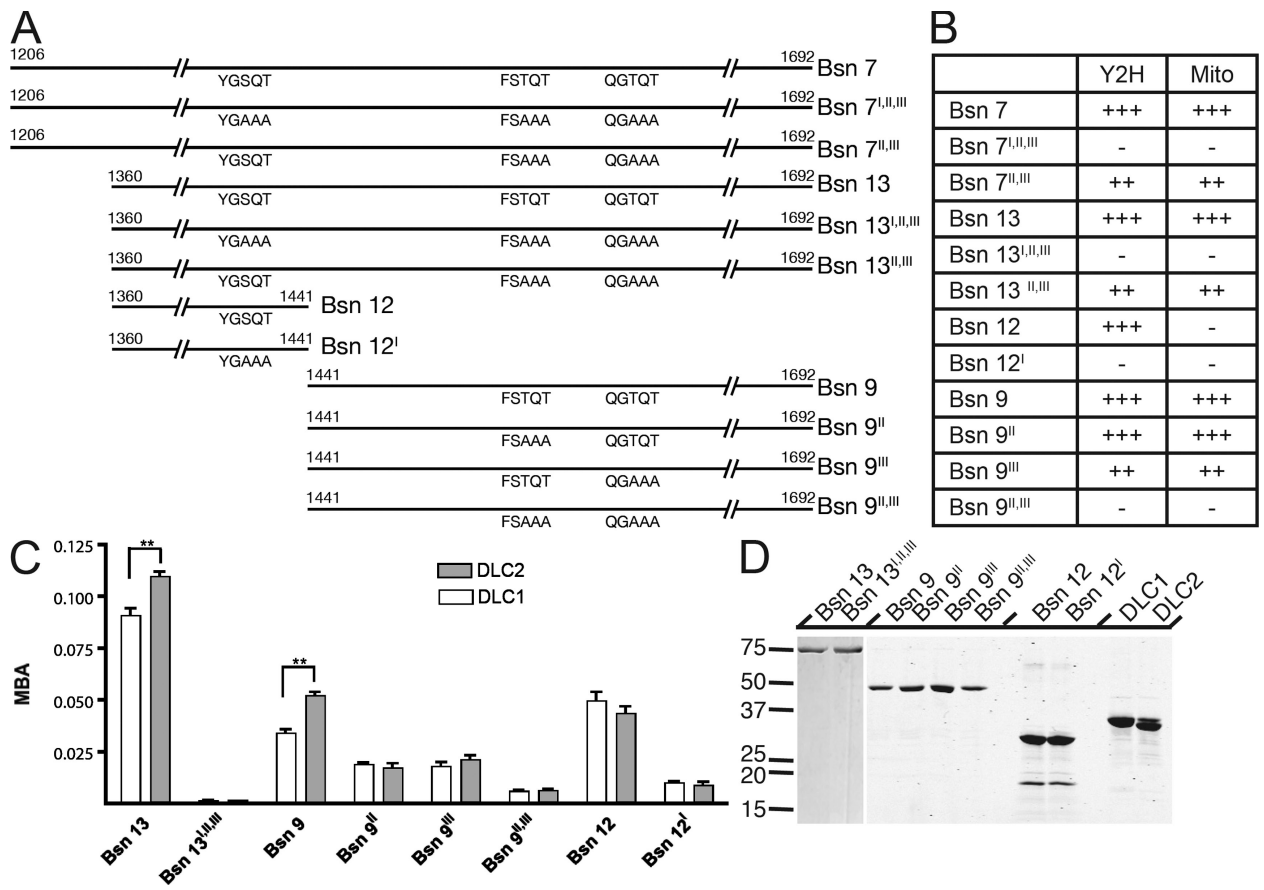

	Y2H	Mito
Bsn 7	+++	+++
Bsn $7^{I,II,III}$	-	-
Bsn $7^{II,III}$	++	++
Bsn 13	+++	+++
Bsn $13^{I,II,III}$	-	-
Bsn 13 ^{II,III}	++	++
Bsn 12	+++	-
Bsn 12^{I}	-	-
Bsn 9	+++	+++
Bsn 9^{II}	+++	+++
Bsn 9^{III}	++	++
Bsn $9^{II,III}$	-	-

Figure 3. **Mapping of three independently functional DLC-binding sites in Bassoon.** (A) Bassoon constructs including the amino acid substitutions introduced at interaction sites I, II, and III and their relative lengths; bordering amino acid numbers refer to rat Bassoon. (B) Summary of binding assays in yeast (yeast two-hybrid [Y2H]) and in corecruitment assay by mito-targeting in COS-7 cells (Mito). (C) Molecular-binding activities (MBA) of purified Bsn fragments to DLC1 and DLC2 in surface plasmon resonance assays. Error bars indicate SEM. **, $P < 0.01$. (D) Recombinant proteins used for the binding assays are shown on a Coomassie-stained SDS gel. Molecular mass is indicated in kilodaltons.

Identification of three functional DLC-binding motifs on Bassoon

Two independent Bassoon regions located on fragments Bsn9 and Bsn12 bind DLCs. To identify the exact DLC-binding site, we screened the amino acid sequence of both regions for sequences similar to published DLC-binding consensus motifs (K/R)XTQT (Lo et al., 2001) and GIQVD (Liang et al., 1999; Fan et al., 2001). Two TQT motifs are present in the sequence of the Bsn9 fragment. Short constructs with the sequences ATAEFSTQTP and PMVAQGTQT, covering the first and second TQT motifs, respectively, can indeed bind DLC in yeast. The respective mutant constructs with TQT motifs replaced by AAA did not bind DLC in this assay (Fig. 3, A and B). To verify that there are no additional DLC-interacting sequence motifs in Bsn9, we generated mutants in which the first ($Bsn9^{II}$), the second ($Bsn9^{III}$), or both ($Bsn9^{II,III}$) TQT motifs were replaced by AAA (Fig. 3 A). Yeast two-hybrid analysis showed that the mutation of both binding motifs was necessary and sufficient to disrupt the interaction between Bsn9 and DLC1 or DLC2. Assessment of colony number and size suggested that DLC binding of $Bsn9^{III}$ is impaired to a greater degree than that of $Bsn9^{II}$, which showed binding basically undistinguishable from Bsn9. Fragment Bsn12 contains an SQT motif instead of the canonical TQT motif. Construct $Bsn12^{I}$, in which SQT was replaced by AAA, was unable to bind DLC1 or DLC2, indicating that the putative DLC-binding motif present in this fragment was inactivated by the mutation. Of note, the replacement of the central Gln residue by Ala in all identified motifs only partially disrupted DLC binding (unpublished data).

Next, we tested whether each of the three DLC-binding sites is sufficient to mediate binding to Bassoon by means of the mitochondrial corecruitment assay. As expected, fragment Bsn9 was recruited to mitochondria when coexpressed with Mito-EGFP-DLC1 (Fig. S2, C and D) or Mito-EGFP-DLC2 (not depicted). The mutation of both TQT motifs disrupted the recruitment of $Bsn9^{II,III}$ but not of construct $Bsn7^{II,III}$, which still contained the SQT motif functioning as the DLC interaction interface. Additional mutation of this motif (in $Bsn7^{I,II,III}$) completely disrupted DLC binding of this fragment. Construct Bsn12, which exhibited binding in yeast, was not recruited to mitochondria in COS-7 cells expressing Mito-EGFP-DLC1 or Mito-EGFP-DLC2, presumably as the result of steric hindrance. The results of the yeast two-hybrid and corecruitment assays in COS-7 cells are tabulated in Fig. 3 B. To further confirm the importance of identified binding motifs, EGFP-Bsn7, -Bsn9, and -Bsn13 and their mutants EGFP-$Bsn7^{I,II,III}$, -$Bsn7^{II,III}$, -$Bsn9^{II,III}$, and -$Bsn13^{I,II,III}$ were expressed in HEK293T cells and precipitated with anti-GFP antibody. Coprecipitation of

overexpressed and endogenous DLC was detected using an anti-DLC antibody (Fig. 2 G and Fig. S2, A and B), confirming that mutation of all identified motifs is required to disrupt the Bassoon–DLC interaction.

Inspection of the primary structure of Bassoon orthologues in different vertebrate species showed an absolute conservation of the second and third DLC-binding motifs despite the divergence of the adjacent sequences (Fig. S3). The first motif was conserved only in birds and mammals but not in zebrafish. The high degree of conservation throughout vertebrate species suggests that the DLC–Bassoon interaction might be of functional significance.

DLC1 and DLC2 are very similar proteins with 93% sequence identity. However, it has been proposed that they are sequestered to distinct protein complexes, as shown for dynein or myosin V motor complexes (Naisbitt et al., 2000; Puthalakath et al., 2001). To assess a possible preference of the binding sites on Bassoon for the two DLC isoforms, we expressed and purified a set of His-thioredoxin fusion proteins covering the first, second, and third or all three binding motifs (Fig. 3 D) and tested their relative binding affinities to purified GST-DLC1 or GST-DLC2 (Fig. 3 C) using surface plasmon resonance technology. The results did not reveal any binding preference for single motifs, but we observed significantly higher binding of fragments Bsn9 (motifs II and III) and Bsn13 (all three motifs) to GST-DLC2 compared with GST-DLC1 (Fig. 3 C and Fig. S3 B). The assay also confirms that the interaction of Bassoon and DLC is direct. Notably, we observed an increase of the relative binding affinities starting with fragments $Bsn9^{II}$ and $Bsn9^{III}$ (containing one DLC-binding site) to Bsn9 (containing two) and finally Bsn13 (containing three binding sites; Fig. 3 C). Thereby, site I seems to bind more tightly than sites II and III, and the relative binding affinities seem to be additive as DLC binding of Bsn13 represented roughly the sum of that of Bsn9 and Bsn12. In agreement with this set of data, we find decreased amounts of DLC coprecipitating with EGFP-$Bsn7^{II,III}$ compared with EGFP-Bsn7 (Fig. S2 B). These observations imply that the arrangement of three DLC-binding motifs in close proximity facilitates binding of Bassoon to DLC in vivo.

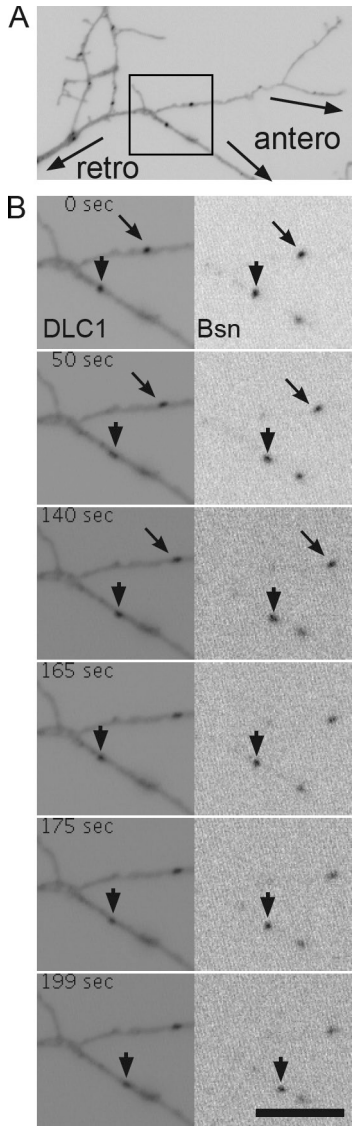

Figure 4. **Co-migration of mRFP-Bsn with DLC1-EGFP.** Cultured neurons were transfected at 3 DIV with DLC1-EGFP and mRFP-Bsn and observed 16 h later by live imaging. (A) Overview image showing a part of an axon with depicted orientation. The black box marks the region enlarged in B, showing co-migration of DLC1-EGFP (left) and mRFP-Bsn (right). Arrows indicate an anterogradely moving particle, and arrowheads indicate a particle with bidirectional movement. See also Video 1. Bar, 5 µm.

Bassoon-transporting vesicles associate with dynein and myosin V

In young neurons, Bassoon is transported into the axon associated with membranous organelles, the PTVs (Zhai et al., 2001; Shapira et al., 2003; Dresbach et al., 2006; Tao-Cheng, 2007). One important cellular function of DLC is linking molecular motors to their cargo. Therefore, we wondered whether Bassoon already associates with DLC during its transport from the cell body toward nascent synapses and whether this interaction might be relevant for Bassoon's delivery to the presynapse. To test this hypothesis, we cotransfected primary neurons with DLC1-EGFP and mRFP-Bsn at 3 d in vitro (DIV) and subjected them to live imaging 1 d later. Co-migration of Bassoon and DLC1-containing fluorescent puncta in both retrograde and anterograde direction (Fig. 4 B and Video 1) suggested cotransport of the two proteins.

In previous imaging experiments, we noted that mobile EGFP-tagged Bassoon puncta migrate in both directions along axons (Bresler et al., 2004), suggesting that anterograde and retrograde motors are involved. Anterograde transport of PTVs relies on kinesin-1 (Cai et al., 2007). In this study, we asked whether Bassoon transport organelles also recruit dynein- and/or myosin V–based motor complexes, both of which contain DLCs. To this end, we enriched PTVs by subcellular fractionation of embryonic brain homogenates (Zhai et al., 2001). Most Bassoon immunoreactivity was found between 0.8 and 1 M sucrose containing synaptic plasma membranes, but significant amounts were also present at the interface between 0.3 and 0.8 M sucrose containing floating PTVs (Fig. 5 A). In both membrane fractions, immunoreactivity was not observed if the samples were preincubated with Triton X-100, confirming that floating of Bassoon depends on its membrane association (Fig. 5 A). Intriguingly, DLC as well as IC74 (the intermediate chain of 74 kD) and

dynein heavy chain (DHC), which are both exclusive components of dynein motor complexes, and myosin V were also detected in the 0.3–0.8 M sucrose interface (Fig. 5 A). Floating of all of these proteins was disrupted upon detergent treatment. This supports the view that Bassoon-carrying PTVs contain both dynein and myosin V motor complexes. To demonstrate conclusively the association of PTVs with multiple motors, we immunoisolated PTVs from the light membrane fraction using the Bassoon-specific monoclonal antibody mab7f (tom Dieck et al., 1998). As shown in Fig. 5 B, DLC, DHC, and myosin V were present in the fraction immunoisolated with mab7f but not with nonspecific IgGs. An antibody recognizing kinesin-1 heavy chains KIF5A/C (subclasses different from KIF5B, which was found on PTVs; Cai et al., 2007) did not detect significant levels of these proteins in the immunoisolated fraction (Fig. 5 B).

To examine the in situ colocalization of endogenous dynein motor complex components and PTVs, we performed immunostainings of neurons at 5 DIV with antibodies against Bassoon, DLC, IC74, and myosin V. A clear colocalization of Bassoon-positive puncta with DLC1/2, IC74, and myosin V was observed (Fig. 5 D). The degree of colocalization of Bassoon, DLC, IC74, and myosin V was quantified by determining the overlap coefficients (OCs) for each stain (Fig. S4) and comparing them with the overlap of Bassoon and cytochrome *c*, which labels mitochondria. The mean OC of costaining for Bassoon and Piccolo (OC = 0.701 ± 0.017; $n = 10$), which is known to be cotransported on the same vesicle, was not significantly different from the OC of costaining for Bassoon with DLC (OC = 0.661 ± 0.019; $n = 21$), IC74 (OC = 0.643 ± 0.015; $n = 19$), or myosin V (OC = 0.755 ± 0.029; $n = 10$). Similarly, the OC of costaining for IC74 and DLC did not differ significantly (OC = 0.6614 ± 0.021; $n = 9$). In contrast, the OC of costaining for Bassoon and cytochrome *c* was significantly lower (OC = 0.496 ± 0.021; $n = 20$; mean ± SEM; $P < 0.0001$). At the analyzed stage (5 DIV), neurons have formed only a few synapses, and the majority of Bassoon is associated with PTVs. Therefore, the colocalization of Bassoon-positive puncta with DLC, IC74, and myosin V in young neurons further supports the notion that these proteins are present on PTVs.

Bassoon can function as a cargo adapter in COS-7 cells and associates with dynein motor complex in neurons

When DLC1 or DLC2 were targeted to the outer mitochondrial membrane in COS-7 cells, the localization of mitochondria was remarkably distinct from that of mitochondria in cells expressing the control construct Mito3-EGFP (Fig. 2, A1, B1, and D1). Normally, mitochondria are distributed throughout the cytoplasm of cells, sometimes even in their most distal regions (Figs. 2 A1 and 6 A1, arrows). In contrast, targeting of DLCs to mitochondria results in their accumulation near the cell center, presumably as the result of DLC-mediated retrograde transport along microtubules via dynein. To test whether Bassoon can function as a cargo adapter, we targeted the fragment Bsn9 to the outer mitochondrial membrane and observed the subcellular localization of mitochondria. After expression of Mito3-EGFP-Bsn9, mitochondria were clustered near the microtubule-organizing center (MTOC) of COS-7 cells, as visualized by costaining of microtubules (Fig. 6, B1 and B2). Targeting of the mutant fragment $Bsn9^{II,III}$, which cannot bind DLC, to mitochondria did not alter their subcellular localization, confirming that an interaction with DLC was required for retrograde transport in COS-7 cells (Fig. 6 C1). Treatment of COS-7 cells expressing Mito3-EGFP-Bsn9 with the microtubule depolymerizing drug nocodazole for 2 h before fixation and staining led to a disruption of clusters, whereas treatment with the actin polymerization inhibitor cytochalasin D had no effect on cluster formation (Fig. 6, D1 and E1). These data suggest that fragment Bsn9 can operate as a cargo adapter via its binding to DLC and induces a microtubule-dependent retrograde transport of organelles in living cells.

To test whether Bassoon associates with the dynein motor complex in neurons, we performed immunoprecipitation experiments from the brain extract of newborn animals. Using Bassoon antibodies, we could coimmunoprecipitate DLC but not other components of the dynein motor complex, (i.e., IC74 or DHC; Fig. 4 C), suggesting that either the interaction is disrupted by the harsh conditions necessary to solubilize Bassoon or the major fraction of cellular Bassoon is not directly associated with motors but still binds DLC. To address this issue further, we immunoprecipitated the dynein motor complex using IC74 antibodies. In this study, significant amounts of Bassoon could be detected in the precipitates together with DHC and DLC (Fig. 5 C), confirming the association of a fraction of Bassoon with the dynein motor complex. Synaptophysin, representing an independent vesicular cargo in the brain at this developmental stage, was not coprecipitated with the dynein motor complex, and unspecific IgGs did not precipitate any of the analyzed proteins.

Mutation of DLC-binding sites in Bassoon affects mobility of PTVs in axons

The physical association of Bassoon with dynein motor complex suggests that the Bassoon–DLC interaction may mediate the trafficking of Bassoon-carrying vesicles within neurons. To test this, a GFP-tagged DLC-binding mutant (DBM) of Bassoon (GFP-BsnDBM) unable to interact with DLC was produced by introducing the aforementioned amino acid exchanges into all three DLC-binding motifs of Bassoon. We observed GFP-Bsn and GFP-BsnDBM particles in neurons transfected at 3 DIV in time-lapse experiments performed 48 h later. At this stage, moderate GFP signals were attained, and bidirectionally moving fluorescent particles could be observed in axons of cells transfected with either construct (Fig. 7 A). This implies that both GFP-Bsn and GFP-BsnDBM were sorted to appropriate transport vesicles. However, during a time period of 32 s (500 frames), a significantly larger fraction of immobile particles was observed in cells expressing GFP-BsnDBM as compared with wild-type Bassoon (72.5 ± 4.1% vs. 53.4 ± 4.1%; mean ± SEM; $n = 6$ cells and 534 and 450 puncta analyzed, respectively; $P = 0.008$; Fig. 7 B and Videos 2 and 3).

To determine velocities and running distances of vesicles carrying GFP-Bsn or GFP-BsnDBM, traces of mobile particles were visualized on kymographs of axonal segments with clear polarity. Traces showing processive movement (without stops and changes in velocities or movement directions) were analyzed.

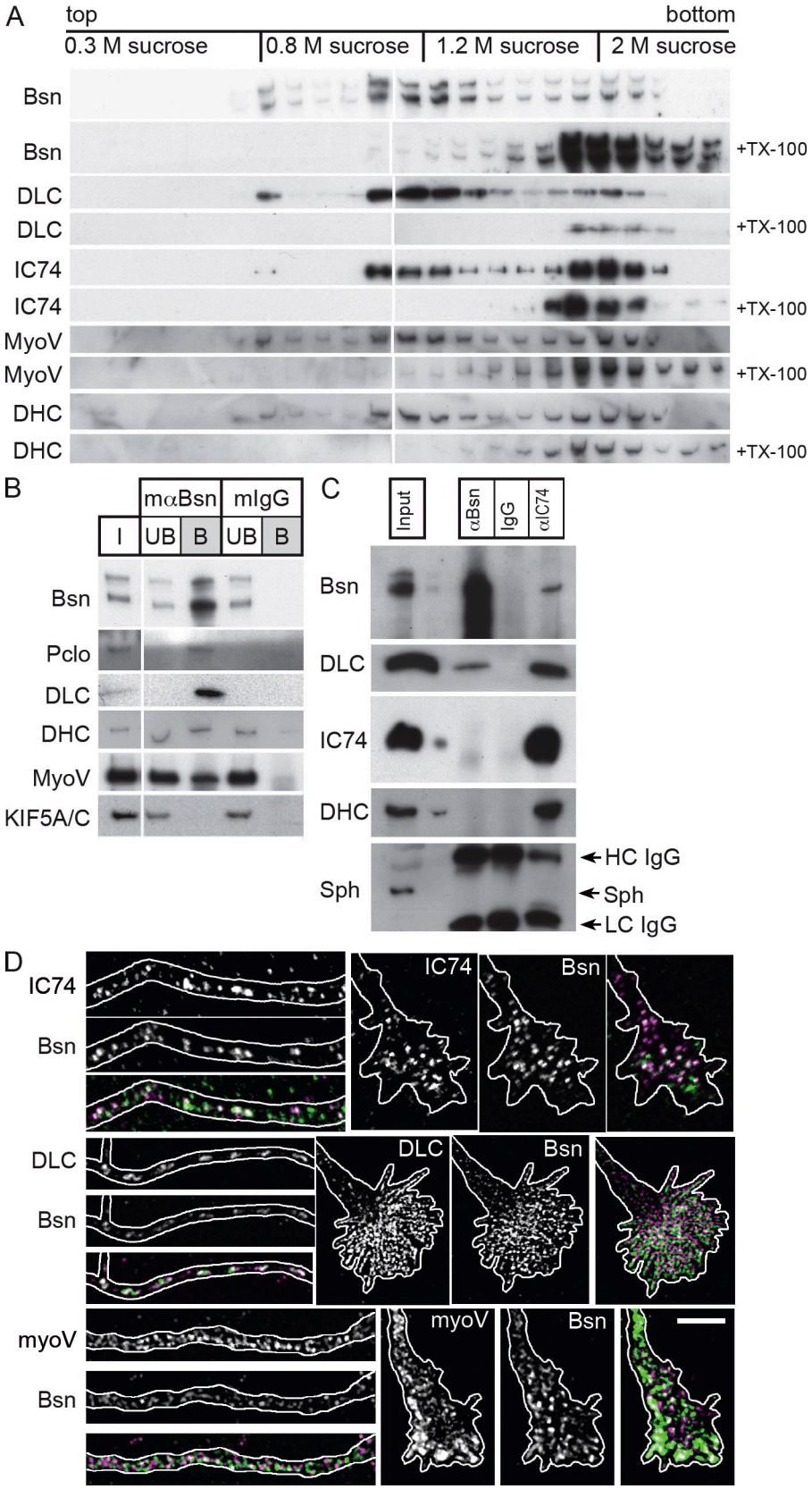

Figure 5. **DLC and other motor components associate with Bassoon transport packets.** (A) Membranes of rat embryonic brain (E18) were subjected to a floatation assay. Equal volumes of each fraction were analyzed on WBs. Membrane association was tested by incubation with the detergent Triton X-100 (+TX-100), which prevents floating of membrane-associated proteins. (B) PTVs were isolated from the light membrane fraction (0.3–0.8 M sucrose) by immunoprecipitation with Bassoon-specific antibodies, solubilized, and probed for their protein content on WBs (mαBsn column). PTV marker proteins Bassoon (Bsn) and Piccolo (Pclo) were detected as well as DLC, DHC, and myosin V (myoV). KIF5A/C was not precipitated at detectable levels. Precipitation with unspecific IgGs (mIgG column) confirmed the specificity of binding. I, input; UB, unbound material; B, bound material. (C) Coprecipitation of protein complexes with anti-Bassoon (αBsn column) and anti-IC74 (αIC74 column) antibody from brain lysate of P1 rats. The presence of DLC in Bassoon-containing complexes as well as the association of Bassoon with assembled dynein motor complex (containing IC74, DHC, and DLC) can be seen. Lanes with input and control precipitations with unrelated IgG are indicated. Synaptophysin (Sph) was not detected in any of the immunoprecipitated complexes. HC, heavy chain; and LC, light chain of coupled antibody. (D) Costaining of Bassoon (magenta) with IC74, DLC1/2, and myosin V (green) in distal axons (left image sequences) and growth cones (right image sequences) of neurons at day 6 after plating. Outlines of axons and growth cones were created according to cell autofluorescences in raw images. Bar, 5 μm.

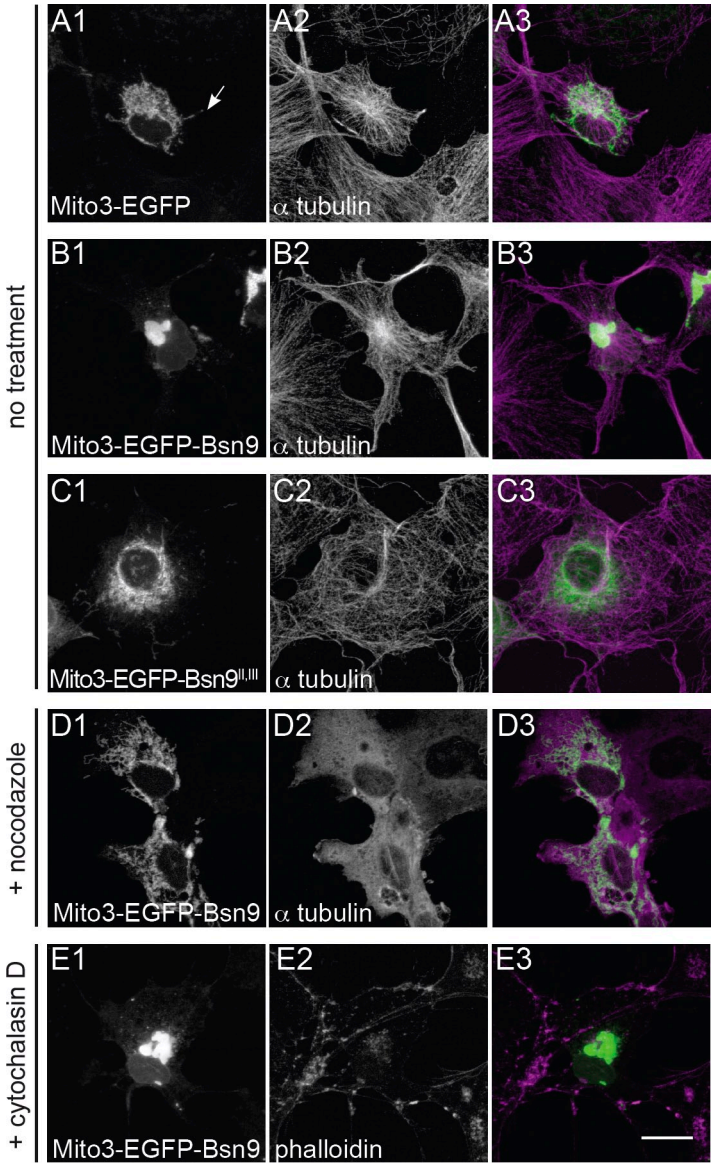

Figure 6. **Bassoon can serve as a cargo adapter for retrograde transport in COS-7 cells.** (A–E) Cells were transfected with mito-targeting constructs and fixed 18 h later. The position of the MTOC is visualized by staining with anti–α-tubulin antibody in A2–D2; actin is visualized with Alexa Fluor 568–coupled phalloidin (E2). In cells expressing mito-targeted fragment Bsn9 containing the DLC-binding sites II and III, mitochondria accumulate at the MTOC. Mitochondria are distributed throughout the cytoplasm in cells expressing mito-targeted EGFP (row A), fragment $Bsn9^{II,III}$ with mutated DLC-binding sites (row C), or in cells expressing mito-targeted Bsn9 after treatment with nocodazole for 2 h before fixation (row D). Depolymerization of actin filaments with cytochalasin D (2 h before fixation) does not prevent the effect of Bsn9 (E1–E3). Bar, 20 µm.

The analysis showed that mutation of the DLC-binding sites in GFP-BsnDBM led to significant decrease in its running distances in both directions compared with GFP-Bsn (retrograde, 1.632 ± 0.1351 µm vs. 2.854 ± 0.2165 µm; mean ± SEM; $n = 10$ cells; 402 vs. 725 traces, respectively; $P < 0.0001$; and anterograde, 1.374 ± 0.09121 µm vs. 2.030 ± 0.1759 µm; $n = 10$ cells; 388 vs. 688 traces, respectively; $P < 0.0005$; Fig. 7 C). Interestingly, a plot of the relative frequency distribution of running distances for GFP-BsnDBM shows a higher proportion of short (<0.5 µm) and a lower proportion of long (>4.5 µm) runs compared with GFP-Bsn ($P < 0.001$ in two-way analysis of variance of cumulative frequency distribution; Fig. 7 E, arrows). The mean velocities of processive movements were also decreased for GFP-BsnDBM compared with GFP-Bsn in both retrograde (0.6727 ± 0.03334 µm/s vs. 1.102 ± 0.04041 µm/s; mean ± SEM; $n = 10$ cells; 402 vs. 725 traces, respectively; $P < 0.0001$) and anterograde (0.6410 ± 0.02972 µm/s vs. 0.8873 ± 0.03549 µm/s; mean ± SEM; $n = 10$ cells; 388 vs. 688 traces, respectively; $P < 0.0001$) movements (Fig. 7 D). These differences in overall mobility and movement characteristics imply that Bassoon's interaction with DLC regulates its axonal trafficking in neurons.

Interaction with DLC controls CAZ protein levels at the synapse

The impaired trafficking of GFP-BsnDBM in the live imaging experiments suggests that the inability to bind DLC might affect the supply of GFP-BsnDBM to synapses. To test this, we analyzed the localization of GFP-BsnDBM in relation to the endogenous pre- and postsynaptic markers synapsin and PSD-95 in 15-DIV neurons (Fig. 8 A). 98.8 ± 0.4% (mean ± SEM) of GFP-BsnDBM fluorescent puncta colocalized with synapsin, and 87.2 ± 2.5% colocalized with PSD-95. This was not significantly different from the localization of GFP-Bsn, where 94.5 ± 2.6% and 82.4 ± 2.8% fluorescent puncta colocalized with synapsin and PSD-95, respectively. Thus, the DLC-binding motifs of Bassoon are not absolutely required for its synaptic targeting.

In further experiments, we interfered with the Bassoon–DLC interaction by overexpressing fragment Bsn9, which includes

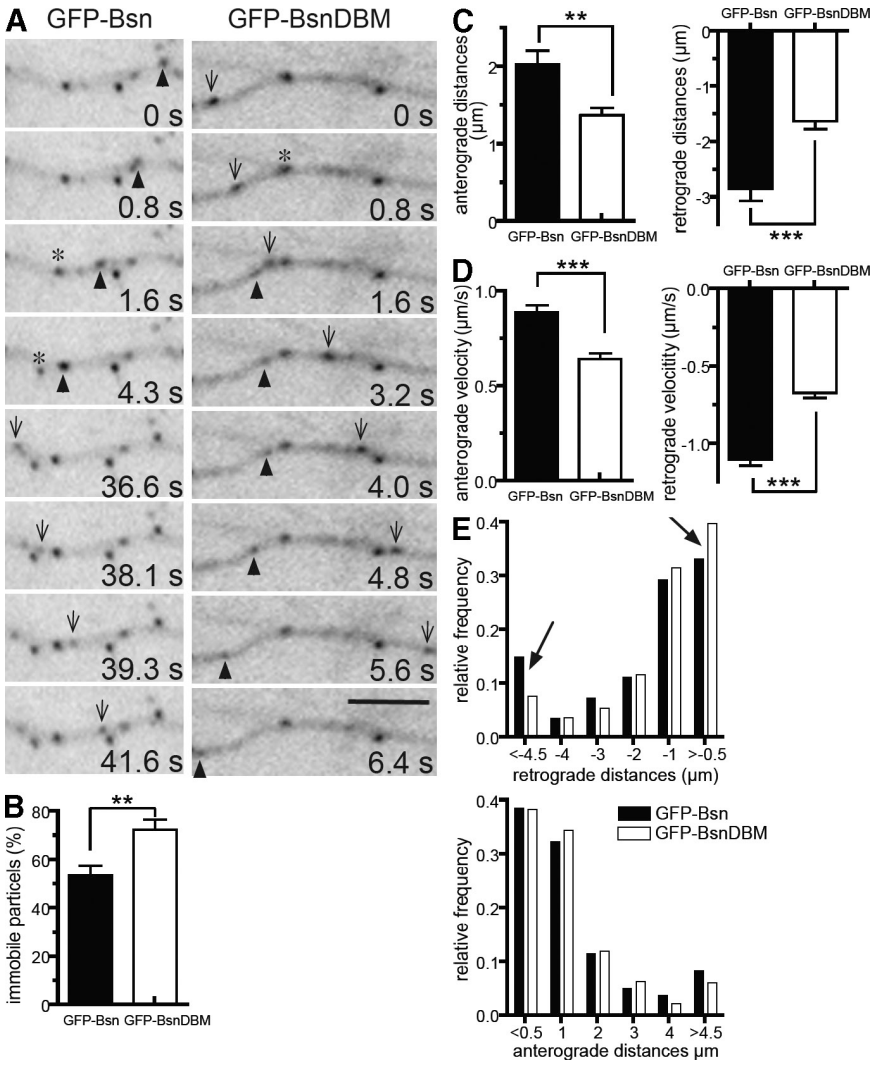

Figure 7. **Axonal trafficking of GFP-Bsn– and GFP-BsnDBM–labeled transport packets.** (A) Axonal segments of 5-DIV neurons transfected 2 d earlier with GFP-Bsn or GFP-BsnDBM. Both GFP-Bsn and GFP-BsnDBM move in both directions (arrowheads and arrows). Asterisks indicate an initially immobile fluorescent particle. (B–D) Graphs showing comparisons of immobile particles (B) and running distances (C) and velocities (D) of anterogradely and retrogradely moving particles in cells transfected with either GFP-Bsn or GFP-BsnDBM. Error bars indicate SEM. **, $P < 0.01$; ***, $P < 0.001$. (E) Relative distribution plot of running distances of GFP-Bsn and GFP-BsnDBM in retrograde and anterograde direction. Note the increased fraction of short retrograde movements (>−0.5) and the decreased fraction of long retrograde movements for GFB-BsnDBM compared with GFP-Bsn (arrows). In all graphs, shaded bars represent GFP-Bsn, and open bars represent GFP-BsnDBM. Bar, 5 µm.

DLC-binding sites II and III. This fragment was able to efficiently pull down DLC from brain lysates (Fig. S5 A). Moreover, trafficking of GFP-Bsn when coexpressed with the Bsn9 fragment (Fig. S5, B and C) very much resembled that of GFP-BsnDBM. To assess the impact of DLC-dependent Bassoon transport on its synaptic delivery, we analyzed amounts of synaptic proteins in 9-DIV neurons when many synapses are newly formed. To this end, we expressed Bsn9 together with EGFP-synapsin translated from the same bicistronic transcript to identify synapses formed by transfected neurons. The relative synaptic amounts of Bassoon were determined as the intensity of immunostaining normalized to mean Bassoon immunoreactivity of synapses formed by axons of nontransfected neurons in the same image. The relative synaptic amounts of Bassoon in cells expressing fragment $Bsn9^{II,III}$ (lacking the DLC-binding sites) with EGFP-synapsin were used as a reference. Thus, effects related to EGFP-synapsin overexpression or to the overexpression of functional elements encoded by Bsn9 that are not related to DLC binding were excluded. The quantitative analysis revealed a significant increase in mean amounts of Bassoon (1.75 ± 0.02 [n = 3,141] vs. 1.50 ± 0.02 [n = 1,827]; mean ± SEM; $P < 0.0001$; Fig. 8 B) and Piccolo (1.57 ± 0.03 [n = 1,420] vs. 1.21 ± 0.02 [n = 1,487]; mean ± SEM; $P < 0.0001$; Fig. 8 C) at synapses of neurons transfected with dominant-negative Bsn9 compared with $Bsn9^{II,III}$. Notably, the relative intensities of Bassoon and Piccolo were much more variable between individual synapses compared with the control situation (Fig. S5, E, F, K, and L). Interestingly, synaptic levels of Munc13, a CAZ protein that can be transported to nascent synapses independently of PTVs (unpublished data), remained unaffected (1.47 ± 0.03 [n = 1,417] vs. 1.43 ± 0.03 [n = 1,038]; mean ± SEM; $P = 0.23$; Fig. 8 D). The amount of postsynaptic PSD-95 was also unchanged (1.40 ± 0.03 [n = 1,372] vs. 1.33 ± 0.03 [n = 1,441]; mean ± SEM; $P = 0.07$; Fig. 8 E). Surprisingly, synaptic levels of synaptophysin (1.568 ± 0.02707 [n = 2,109] vs. 1.712 ± 0.02689 [n = 2,399]; mean ± SEM; $P = 0.0002$; Fig. 8 F) and vGLUT1 (2.083 ± 0.05944 [n = 720] vs. 2.429 ± 0.07300 [n = 772]; mean ± SEM; $P = 0.0003$; Fig. 8 G) were slightly but significantly reduced upon overexpression of Bsn9 (Fig. S5, I, J, O, and P).

Discussion

We report a novel interaction between the presynaptic active zone protein Bassoon and DLC1 and DLC2. We identified three independently functioning DLC-binding sites in Bassoon and

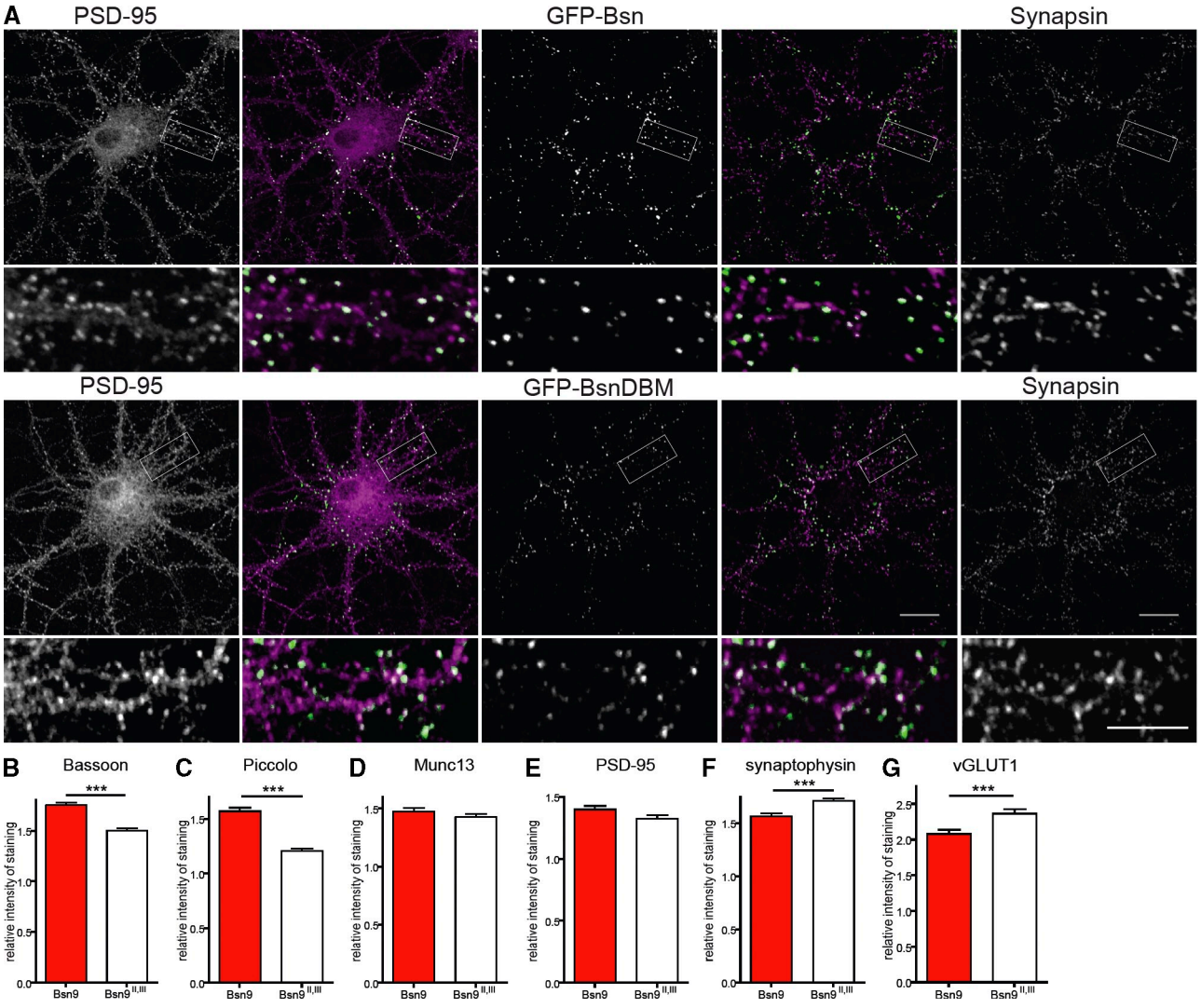

Figure 8. **Overexpression of dominant-negative fragment Bsn9 enhances accumulation of Bassoon and Piccolo at synapses.** (A) Cells transfected at 3 DIV with GFP-Bsn (top) and GFP-BsnDBM (bottom) were fixed at 15 DIV and counterstained to visualize synapsin (last image in each row and magenta in merged image) and PSD-95 (first image in each row and magenta in merged image). The fluorescence of GFP fusion proteins is shown in the middle image of each row (green in merged images). The second and fourth panels are merged images of panels to their right and left. Higher magnifications of the boxed regions are shown below the respective image. (B–G) Quantification of relative staining intensities for Bassoon (B), Piccolo (C), Munc13 (D), PSD-95 (E), synaptophysin (F), and vGLUT1 (G) in cells transfected at 3 DIV with the bicistronic construct expressing EGFP-synapsin and Bsn9 (red bar) or control fragment $Bsn9^{II,III}$ (open bar) and analyzed at 9 DIV. Bar graphs show mean values of relative fluorescence intensity for each staining, and error bars indicate SEM. Values are derived from three independent experiments. ***, $P < 0.001$. Bars: (A) 20 µm; (insets) 10 µm.

showed that these could function in linking cargo to the dynein motor complex in vivo. Interfering with the DLC–Bassoon interactions affects the trafficking of PTVs and the distribution of Bassoon and the related protein Piccolo among synapses, resulting in an increased variability in the Bassoon and Piccolo content of individual presynaptic boutons.

Three functional DLC-binding sites on Bassoon

We identified three independently functional DLC-binding sites on Bassoon, all resembling but not exactly matching the DLC-binding consensus sequence (K/R)XTQT (Lo et al., 2001). This is in line with the previously reported high diversity of binding sites identified among known DLC-interacting partners (Lajoix et al., 2004). Notably, none of three DLC-binding sites of Bassoon is conserved in its paralogue Piccolo. Mutated Bassoon fragments, in which the essential (T/S)QT motifs were replaced by AAA, did not interact with DLCs neither in biochemical assays nor in yeast or mammalian cells. Therefore, it is likely that Bassoon binds DLCs via the target-interacting groove of DLCs, which is the interaction interface also shared by other known DLC interaction partners (Liang et al., 1999; Fan et al., 2001; Lo et al., 2001). Quantitative in vitro binding assays revealed that all three sites are active, that site I has a higher relative affinity for DLCs than sites II and III, and that binding strengths seem to be additive. Moreover, fragment $Bsn7^{II,III}$, bearing only one DLC-binding motif, coprecipitated DLC from HEK293T cells less efficiently than fragment Bsn7, which bears all three. Thus, the cluster of three DLC-binding motifs constitutes a multivalent interaction interface in Bassoon that is likely to facilitate the DLC–Bassoon interaction.

In agreement with the high homology of DLC1 and DLC2, Bassoon was observed to bind both isoforms. However, quantitative binding assays with Bassoon fragments containing two or three DLC-binding interfaces showed significantly higher affinity for DLC2 than for DLC1. Because of the lack of DLC1- and DLC2-specific antibodies, we were unable to examine binding partner preferences of Bassoon in vivo.

One important cellular function of DLCs is to link their binding partners to dynein- or myosin V–dependent transport processes. In neurons, DLCs were shown to bind postsynaptic scaffold molecules like guanylate kinase-associated phosphatase (Naisbitt et al., 2000) or gephyrin (Fuhrmann et al., 2002), and active retrograde transport was proposed as a mechanism contributing to activity-dependent remodeling of the postsynaptic receptor apparatus (Maas et al., 2006). However, the functional role of DLCs as cargo adapters for dynein motors has become a subject of recent debate (Vallee et al., 2004; Barbar, 2008). The binding of DLC cargoes occurs in the same binding groove as the binding to dynein motor complex via IC74 (Williams et al., 2007). In this configuration, the DLC interaction partners would probably compete with the dynein motor complex for binding to DLC rather than being linked to the dynein motor complex via DLC. In this study, targeting of DLC-binding Bassoon fragments to mitochondria led to their accumulation near the cell center (probably the MTOC). This accumulation was dependent on both intact DLC-binding motifs and assembled microtubules and is best explained by assuming retrograde transport of Bassoon-tagged mitochondria. Similarly, a point mutation of the DLC-binding motif in the protein Egalitarian (Navarro et al., 2004) or deletion mutants of Swallow (Schnorrer et al., 2000) or Dazl (Lee et al., 2006) deficient in DLC binding showed defects in their dynein-mediated transport. In this study, we observed that Bassoon associates with the dynein motor complex in vivo and that the mutation of its DLC-binding motif has profound effects on microtubule-dependent transport when expressed in primary neurons. These findings support the view that Bassoon, via its interaction with DLCs, might function as a cargo adapter for the retrograde motor dynein.

Bassoon links dynein and myosin motors to PTVs

Recent studies established that newly synthesized Bassoon is transported toward nascent synapses associated with Golgi-derived vesicular structures, PTVs (Zhai et al., 2001; Shapira et al., 2003; Dresbach et al., 2006). Imaging studies using GFP-tagged Bassoon revealed that PTVs move along axons in both directions until they stop at sites of synaptogenesis (Shapira et al., 2003; Bresler et al., 2004). Fast long-range transport in axons is achieved by anterograde and retrograde movement of molecular motors along microtubules (Vale, 2003). Recently, the anterograde motor kinesin-1 was reported to link to PTVs via a syntaxin1–syntabulin–KIF5B adapter complex, mediating their transport toward synapses (Su et al., 2004; Cai et al., 2007). As the molecular link to retrograde transport remained unknown, we followed the hypothesis that interaction of Bassoon with DLC might be relevant in this context. Our data suggest that DLCs associate with mobile Bassoon packets, which also contain DHCs possibly linked through DLCs. Accordingly, the retrograde transport of PTVs along microtubules could be driven by the dynein motor complex recruited via Bassoon, although Bassoon is most likely not the only cargo adapter for dynein on PTVs. For example, voltage-dependent Ca channels, which were identified as potential components of PTVs (Shapira et al., 2003) and can interact with the DLC tctex-1 (Lai et al., 2005), might represent such an alternative cargo adapter.

Why are organelles such as PTVs, which are designated for axonal targeting, equipped with both anterograde and retrograde motors when unidirectional anterograde transport might be simpler and more economical? Regulated bidirectional movement of organelles might assure their relative uniform distribution in the outgrowing axon to be available for efficient synapse formation all along the axon.

What might be the physiological role of the Bassoon–DLC interaction in neurons?

To assess whether the Bassoon–DLC interaction links PTVs to microtubule-based axonal transport, the mobility of vesicles carrying either GFP-tagged wild-type Bassoon or DLC binding–deficient Bassoon were compared. Bidirectional movement observed in both cases implies that the perturbed DLC binding does not interfere with the appropriate sorting of Bassoon to transport packages, which are expected to also carry endogenous Bassoon. Nonetheless, a significant decrease in the overall mobility of GFP-BsnDBM–bearing vesicles as compared with GFP-Bsn–carrying vesicles was observed. A plausible explanation might be that bidirectional motors are tightly cross-regulated, i.e., when a motor for one direction is disturbed, the opposite motor does not simply take over. This is well demonstrated by mutants of kinesin heavy chain (Goldstein, 2001), kinesin light chain (Gindhart et al., 1998), or DHC (Martin et al., 1999), which result in the accumulation of their respective cargoes in axons but not strictly in their accumulation in the cell body or in distal part of axons. Moreover, it was hypothesized that the presence of multiple classes of motor proteins on one vesicle might cooperate to avoid collision when two vesicles are transported in opposite direction on the same microtubule track (Welte, 2004). Thus, the increased number of immobile particles may reflect the predisposition of Bassoon particles with perturbed links to dynein motor complexes to be involved in "traffic jams" on microtubule tracks.

The analysis of vesicle movements in retrograde and anterograde directions revealed significant decreases in retrograde and anterograde velocities as well as in running distances in both directions for DLC binding–deficient Bassoon compared with the wild-type GFP-Bassoon. Effects on the anterograde transport by interference with components of retrograde molecular motors like DHC or dynactin have also been reported in previous studies (Gross et al., 2000, 2002; He et al., 2005). This has been attributed to the necessity of efficient coordination of opposite-polarity motors by one another.

Despite the numerous immobile vesicles seen at 5 DIV in neurons expressing GFP-BsnDBM, normal localization of the construct with respect to pre- and postsynaptic markers was observed at 14 DIV, when synaptogenesis declines and PTVs are

reduced in cultured neurons (Zhai et al., 2000). However, interference with the Bassoon–DLC interaction leads to significant increase in mean Bassoon and Piccolo levels at individual synapses of transected neurons compared with controls. DLC-mediated transport of Bassoon and Piccolo away from synapses might be part of a protein exchange process fine-tuning synaptic amounts of these proteins (Tsuriel et al., 2006, 2009). Furthermore, our analysis revealed a striking increase in variability of both Bassoon and Piccolo contents at individual synapses. This confirms that the transport of both proteins is tightly linked and suggests that interference with Bassoon's interaction with DLC causes a defect in the trafficking of their common carrier.

It was proposed that synaptogenesis occurs in two phases. Initially, SV precursors traveling along microtubule tracks pause or stop at locations predefined by yet unknown mechanisms. This leads to the formation of "orphan" transmitter release sites that can accumulate active zone proteins (Krueger et al., 2003; Sabo et al., 2006). In the second step, the initially formed site can split, and release-capable packages containing SVs and active zone material start to travel bidirectionally along axons (Krueger et al., 2003). Thus, the primary capturing of presynaptic scaffold molecules can occur at nascent synaptic sites in a random fashion. Their subsequent bidirectional active distribution among adjacent synaptic boutons might represent a mechanism assuring formation of a rather homogeneous synapse population. In line with this hypothesis, PTVs, after interference with Bassoon–DLC interactions, are stranded at the places where their transport paused because they cannot be transported further as a result of their impaired capacity to bind dynein. The high variance in synaptic levels of Bassoon and Piccolo could reflect the inability to more evenly redistribute the stochastically deposited clusters of PTVs during initial phases of synaptogenesis.

The levels of SV proteins synaptophysin and vGLUT1 were decreased in synapses of neurons overexpressing the DLC-capturing fragment Bsn9. The actual reason for this observation is currently unclear. As Piccolo was recently identified to negatively regulate SV exocytosis (Leal-Ortiz et al., 2008), the decrease of SV markers might be caused by increased levels of Piccolo. In the dominant-negative approach achieved by overexpression of Bsn9, synaptic levels of the CAZ protein Munc13 were not changed. This argues that interference with the Bassoon–DLC interaction did not have a general pleiotropic effect on axonal transport and is in line with described mechanisms of Munc13 synaptic targeting. Munc13 is recruited to synapses via the Rab3-interacting molecule (Andrews-Zwilling et al., 2006), which, in turn, is localized to synapses depending on the presence of CAZ-associated structural protein/ERC2 (Ohtsuka et al., 2002). Synaptic targeting of CAZ-associated structural protein is partly independent from Bassoon, which is consistent with the finding that it is not transported exclusively on PTVs (Ohtsuka et al., 2002). Preliminary experiments confirm that specific blockade of Bassoon's exit from the trans-Golgi network does not disrupt the transport or appearance of Munc13 at synapses (unpublished data).

The amount of the postsynaptic marker PSD-95 also remained unchanged. As the size of pre- and postsynaptic elements is tightly coregulated (Schikorski and Stevens, 1999), additional Bassoon and Piccolo molecules detected in a subpopulation of synapses after expression of dominant-negative Bsn9 might not be inserted into presynaptic plasma membrane but accumulate within the presynaptic bouton. Perhaps PTVs are affected, after they dissociate from microtubules in synaptic areas, in their switch to myosin V driving their transport toward the presynaptic plasma membrane along actin filaments. Our immunostaining and immunoprecipitation experiments of PTVs confirm an association of myosin V with PTVs. Whether this switch from microtubule- to actin-based motors also involves DLC–Bassoon interactions will be the subject of future investigations.

Altogether, our experiments have shown that Bassoon interacts with DLCs in neurons, that this interaction is essential for proper movement of Bassoon transport packets along the axon, and that disruption of the interaction affects the accurate distribution of the CAZ scaffolding proteins Piccolo and Bassoon to the sites of neurotransmitter release.

Materials and methods

Cloning of constructs

The pMito3-EGFP vector was generated by introducing aa 1–33 of rat TOM20, coding for its mitochondrial targeting signal (Kanaji et al., 2000), into a eukaryotic expression vector, which was derived from pCMV-Tag3A (Agilent Technologies) by excision of the myc tag. The EGFP coding sequence was subsequently inserted in frame at the 3′ end of the TOM20 sequence. The GFP-Bsn construct used in this study was described previously as GFP-Bsn95-3938 (Dresbach et al., 2003), and the mRFP-Bsn construct, in which GFP was replaced by mRFP, is its analogue. Cloning of Bsn1–4 fragments was described previously (Dresbach et al., 2003). All other Bassoon and Piccolo constructs were generated using PCR with extended primer, thereby adding BamHI and XhoI restriction sites at the 5′ and 3′ ends of the fragments, respectively. The introduced restriction sites were used for in-frame cloning of fragments into the vectors pGADT7, pGBKT7, pEGFP-C2 (Clontech Laboratories, Inc.), pMito3-EGFP, and pmRFP-C2, which was constructed by introducing the mRFP sequence (gift from R.Y. Tsien, University of California, San Diego, La Jolla, CA) instead of the EGFP sequence into the pEGFP-C2 plasmid. The coding sequence of DLC1, flanked at its 5′ end with EcoRI and at its 3′ end with XhoI sites, was generated by PCR using extended primers. Accordingly, the coding sequence of DLC2 was flanked with BamHI (5′ end) and XhoI (3′ end). The introduced restriction sites were used for in-frame cloning of fragments into the plasmids pGADT7, pGBKT7, pCMV-Tag2C (Agilent Technologies), pMito3-EGFP, pEGFP-N1 (Clontech Laboratories, Inc.), and pGEX-5X (GE Healthcare). The His-Strep expression vector pETS-32a$^+$ was generated by ligation of a Strep-tagII (IBA) encoding synthetic DNA fragment with 5′ XhoI and 3′ SalI into the XhoI site of the plasmid pET-32a$^+$ (EMD). Bassoon fragments were cloned into the multiple cloning site of the resulting plasmid using appropriate restriction sites. Short fragments coding for the second and third DLC-binding interfaces of Bassoon were constructed by in-frame insertion of synthetic oligo-deoxynucleotides coding for the respective sequence into pGADT7 or pGBKT7 vectors. All mutations described were introduced by inverse PCR using primers with mutated sequence and corresponding Bassoon fragments subcloned in pBluescriptII SK$^-$ (Agilent Technologies) as a template. cDNA of EGFP-synapsinIa was a gift from T.A. Ryan (Cornell University, New York, NY).

Yeast two-hybrid experiments

For cDNA library screening, the Matchmaker Two-Hybrid System 2 (Clontech Laboratories, Inc.) was used with a rat brain Matchmaker cDNA library (Clontech Laboratories, Inc.) as prey and Bassoon fragment Bsn2 as bait. Transformation and selection was performed according to the manufacturer's protocols. For narrowing down the DLC interaction region in Bassoon and for interaction analysis of Piccolo and mutated Bassoon construct, the Matchmaker system 3 (Clontech Laboratories, Inc.) was used. In detail, the Bassoon and Piccolo constructs based on pGBKT7 were cotransformed with DLC1 or DLC2 in pGADT7 vectors into AH109 yeast cells using standard transformation protocols. Cotransformed cells were selected by growth on Leu- and Trp-lacking medium. The interaction of coexpressed proteins

activating expression of reporter genes was monitored as growth on selection media lacking adenine, His, Leu, and Trp and supplemented with 1 mM 3-amino-1,2,4-triazole after 4 and 7 d. Potential self-activation of constructs was always tested in parallel by cotransformation with empty prey or bait vectors. Constructs Bsn7, Bsn9, and Bsn13 and Pclo1 and Pclo2 constructs covering aa 1,918–2,469 and aa 1,918–2,204 were self-activating in pGBKT7. Therefore, they were subcloned into pGADT7 and tested with DLC1 or DLC2 cloned in pGBKT7.

Biosensor analysis

GST- and His-tagged fusion proteins were expressed and purified by affinity chromatography using glutathione Sepharose 4 Fast Flow (GE Healthcare) or HisPur cobalt resin (Thermo Fisher Scientific) according to the manufacturer's recommendation. Strep-His fusion proteins were purified by double-step chromatography using HisPur matrix (Thermo Fisher Scientific) and Strep-Tactin Superflow (IBA). The purified proteins were dialyzed against PBS before biosensor analysis. All experiments were performed using a Biacore 2000 (Biacore) and a sensor chip (CM5; Biacore) at 25°C. The active surface (with immobilized anti-GST antibody) was prepared using the Amine Coupling kit (Biacore) combined with the GST Capture kit (Biacore) according to the procedure recommended by the manufacturer. Binding GST-DLC1, GST-DLC2, and GST as control was performed in HBS-EP (0.01 M Hepes buffer, pH 7.4, and 0.15 M NaCl with 0.005% surfactant P20) running buffer at a concentration of 20 µg/ml and a flow rate of 20 µl/min for 6 min. Soluble ligands (Bassoon fragments) were applied in HBS-EP running buffer containing 0.105% surfactant P20 at a concentration of 20 µg/ml at a flow rate 20 µl/min for 6 min. The parallel application of soluble ligand to the GST reference cell allowed controlling for nonspecific binding. The surface was regenerated using 10 mM Gly-HCl, pH 2.2, for 2 min at 20 µl/min. To standardize the results of measurements using ligands with different molecular masses, the molecular-binding activities (MBA) were calculated according to the equation

$$\mathrm{MBA} = \frac{(\text{ligand response}) \times (\text{molecular mass of receptor})}{(\text{amount of receptor}) \times (\text{molecular mass of ligand})}$$

(Catimel et al., 1997).

Antibodies and stains

The following antibodies were used: rabbit antibodies against DLC (DLC8; diluted 1:40,000 for WBs and 1:1,000 for immunocytochemistry [ICC]; Abcam), DLC1/2 (diluted 1:1,000 for ICC; gift from M. Sheng, Massachusetts Institute of Technology, Cambridge, MA; Naisbitt et al., 2000), synaptophysin (diluted 1:5,000 for ICC; gift from R. Jahn, Max Plank Institute for Biophysical Chemistry, Göttingen, Germany), Bassoon (sap7f; diluted 1:2,000 for ICC; tom Dieck et al., 1998), GFP (diluted 1:10,000 for WBs; Abcam), myosin V (diluted 1:1,000 for ICC; Sigma-Aldrich), Munc13-1 (diluted 1:1,000 for ICC; Synaptic Systems GmbH), and synapsin (diluted 1:2,000 for ICC; Synaptic Systems GmbH). Mouse antibodies used were against cytochrome *c* (diluted 1:100 for ICC; BD), IC74 (diluted 1:2,000 for WBs and 1:50 for ICC; Millipore), Flag M2 (diluted 1:10,000 for WBs; Sigma-Aldrich), kinesin heavy chain (H2; diluted 1:2,000 for WBs; Millipore), c-myc (9E10; diluted 1:1,000 for WBs; Santa Cruz Biotechnology, Inc.), α-tubulin (diluted 1:1,000; Sigma Aldrich), synapsin (diluted 1:2,000 for ICC; Synaptic Systems GmbH), PSD-95 (diluted 1:1,000–2,000 for ICC; Millipore), and Bassoon (mab7f; diluted 1:2,000 for WBs and 1:1,000 for ICC; Assay Designs). Other antibodies used were from goat against DHC (S19; diluted 1:200 for WBs; Santa Cruz Biotechnology, Inc.), from guinea pig against Piccolo (diluted 1:1,000–2,000 for WBs and ICC; Dick et al., 2001), and from rat against DLC (diluted 1:500 for WBs; Enzo Biochem, Inc.). MitoTracker red CMXRos, MitoTracker deep red 633 (200 nM final concentration), and phalloidin–Alexa Fluor 568 (diluted 1:500 for ICC) were purchased from Invitrogen, and Alexa Fluor 488–, Cy3-, Cy5-, and peroxidase-coupled antibodies were purchased from Jackson ImmunoResearch Laboratories.

Corecruiting assay in COS-7 cells, immunostaining, and immunoprecipitation

Transfection of COS-7 cells grown on glass coverslips coated with poly-D Lys was performed using the transfection reagent Polyfect (QIAGEN) according to the manufacturer's instructions. To label mitochondria, cells were treated with MitoTracker reagent as described previously (tom Dieck et al., 2005). Cells were fixed in 4% paraformaldehyde and 4% sucrose in PBS, pH 7.4, for 5 min at RT. Before immunostaining, blocking was performed for 1 h in PBS containing 10% FCS, 0.1% Gly, and 0.3% Triton X-100. Primary and secondary antibodies were diluted in PBS containing 3% FCS. Images were taken with a confocal microscope (SP2; Leica) equipped with LCS software (Leica) or with an upright microscope (Axioplan2; Carl Zeiss, Inc.) equipped with a camera (Spot RT-KE; Diagnostics Instruments, Inc.) and MetaVue software (MDS Analytical Technologies). Nocodazole and cytochalasin D (both from EMD) were used in concentrations of 10 µM, and 1 µM, respectively. HEK293T cells grown in 75-cm^2 flasks were transfected using the Ca phosphate method. In brief, 0.5 ml of 0.5 M $CaCl_2$ were mixed with 25 µg DNA (for double transfection; 12.5 µg of each DNA). Then, 0.5 ml of 140 mM NaCl, 50 mM Hepes, and 1.5 mM Na_2PO_4, pH 7.05, were added and, after 1 min, and applied to cells in culture. The cells were incubated for 4 h at 37°C in 5% CO_2 atmosphere before exchange of growth media. Cells were lysed in 50 mM Tris-HCl, pH 7.4, 0.5% Triton X-100, 100 mM NaCl, 10% glycerol, 1.5 mM $MgCl_2$, and complete protease inhibitors (Roche) for 15 min on ice 48 h after transfection. Cleared cell lysate was used for immunoprecipitation using MicroMACS anti-GFP MicroBeads and MicroColumns (Miltenyi Biotec) according to the manufacturer's instructions, but using lysis buffer in all washing steps.

Light brain membrane preparation, immunoisolation of Bassoon-containing vesicles, and immunoprecipitation of Bassoon and the dynein motor complex

Light membrane preparation and vesicle immunoisolation were preformed as described previously (Zhai et al., 2001), with minor modifications. Embryonic day (E) 18 brains were homogenized in 5 mM MES, pH 7.0, 1 mM EDTA, and 0.32 M sucrose with complete protein inhibitors. The homogenate was centrifuged at 1,500 *g* for 20 min, and crude membranes in the supernatant were lysed hypotonically by adding 9 vol of homogenization buffer without sucrose. The crude membrane extract was then centrifuged at 100,000 *g* for 1 h. The pellet was resuspended in homogenization buffer with 2 M sucrose and loaded as a layer of a discontinuous sucrose gradient underneath layers of 1.2, 0.8, and 0.3 M sucrose. The sucrose gradient was spun for 3 h at 350,000 *g*. Fractions were taken from the top of the gradient to the bottom. Immunoisolations were performed with superparamagnetic beads (Dynabeads Protein G; Invitrogen) according to the manufacturer's protocol. In brief, mab7f or unspecific IgGs (50 µg/100 µl of beads) were bound to beads for 2 h at RT and, after being washed three times with PBS, were cross-linked using dimethyl pimelimidate. Beads were collected using a magnetic device (Dynal MPG; Invitrogen). Dynabeads coupled with specific antibodies or IgGs were incubated with light membrane fraction (collected at 0.3–0.8 M sucrose interface) overnight at 4°C. Beads were then extensively washed (PBS, 0.1% Tween 20, and 3% FCS), and immunoisolated vesicles were eluted in SDS loading buffer.

Immunoprecipitation of dynein motor complex was performed as described previously (Dillman and Pfister, 1994), and Bassoon multiprotein complexes were precipitated analogously. In brief, 20 µg of anti-Bassoon (mab7f), anti-IC74 antibody, or normal mouse IgGs were covalently coupled to 50 µl of GammaBind Plus Sepharose beads (GE Healthcare) using dimethyl pimelimidate. Postnatal day (P) 1 rat brains were homogenized in 25 mM Tris-Cl, pH 8.1, 50 mM NaC1, 2 mM EDTA, and 0.5% Triton X-100 plus complete protease and PhosSTOP phosphatase inhibitors cocktail (Roche). After centrifugation at 27,000 *g* for 15 min, the lysate was precleared by incubation with beads for 30 min, diluted 1:1 with NET gel (150 mM NaCl, 5 mM EDTA, 50 mM Tris, pH 7.4, 0.25% gelatin, 0.05% Triton X-100, and complete protease inhibitors cocktail), and, finally, incubated with antibody-coupled beads for 3 h. The beads were washed three times with buffer A (PBS, pH 7.4, 0.5% Triton X-100, 0.05% sodium deoxycholate, 0.01% sodium dodecyl sulfate, and 0.02% sodium azide) followed by three washes with buffer B (125 mM Tris, pH 8.1, 500 mM NaCl, 0.5% Triton X-100, 10 mM EDTA, and 0.02% sodium azide). The precipitates were eluted into SDS loading buffer. Pull-downs were performed using purified Bassoon fragments bound to HisPur cobalt resin using the analogous homogenization and washing procedure as was used for the aforementioned immunoprecipitation experiments.

Neuronal cultures

Dissociated primary hippocampal cultures were prepared as described previously (Frischknecht et al., 2008). Transfection of cultured neurons was performed as described previously (Dresbach et al., 2003). Neurons were fixed in 4% paraformaldehyde and 4% sucrose in PBS, pH 7.4, for 5 min. For staining with the anti-DLC1/2 and anti-IC74 antibody, neurons were fixed by immersion in precooled 100% methanol for 20 min at −20°C. Neurons were immunostained according the same protocol as COS-7 cells.

Live imaging microscopy

Live imaging was performed at 37°C using an inverted microscope (Axio Observer A1; Carl Zeiss, Inc.) in a heated imaging chamber (QE-1; Warner

Instruments) and a camera (QuantEM 512SC; Photometrics) controlled by MetaMorph Imaging software (MDS Analytical Technologies) using a 100× NA 1.3 objective, a monochromator (PolychromeV; TILL Photonics), and a standard GFP or double GFP/mRFP excitation/emission filter set (Chroma Technology Corp.). Time-lapse images were captured every second for imaging of mRFP-Bassoon and DLC1-EGFP co-migration. Stream acquisition mode was used with 33 or 66 frames/s for analysis of the immobile vesicle fraction and with 10 frames/s for analysis of bidirectional vesicle movement characteristics. Experiments were performed under constant perfusion with 119 mM NaCl, 2.5 mM KCl, 2 mM $CaCl_2$, 2 mM $MgCl_2$, 30 mM glucose, and 25 mM Hepes, pH 7.4.

Data analysis

In general, images were adjusted and analyzed using ImageJ (National Institutes of Health), MetaMorph, Photoshop (Adobe), or OpenView software (written by N.E. Ziv; Tsuriel et al., 2006). The analysis of OCs was performed using the JACoP plugin (Bolte and Cordelieres, 2006) of ImageJ. The OC expresses the correlation of pixel intensities in both analyzed channels. It reaches values from 0 to 1, where 0 indicates no overlap at all (complementary images), 0.5 indicates random distribution of staining, and 1 reflects 100% colocalization between both channels. Immobile particles were determined as the percentage of particles that did not change their position within the analyzed time frame (32 s corresponding to 500 frames) relative to the total detected fluorescent particles. To measure velocities and distances of traces with processive movements, kymographs were created and analyzed using MetaMorph software. For analysis of fluorescence intensities of individual synapses, maximal projections of confocal stacks were created, and synapse detection, matching, and intensity measurement in all analyzed channels were performed using a semiautomatic routine based on OpenView software. The staining intensity of each transfected synapse was normalized to the mean intensity of nontransfected synapses in the same image field. All statistical analyses were performed with Prism 4 software (GraphPad Software, Inc.).

Online supplemental material

Fig. S1 shows a map of pMito3-EGFP and the colocalization of Mito3-EGFP fusion proteins with MitoTracker in COS-7 cells. Fig. S2 shows additional results of coprecipitation experiments with EGFP-Bsn7, -Bsn9, and -Bsn13 and their point mutants and a mito-targeting assay with Bsn9. Fig. S3 shows how the DLC-binding motifs are conserved among Bassoon orthologues and numerical values of biosensor analysis using DLC1, DLC2, and Bassoon fragments. Fig. S4 shows quantitative colocalization analysis of Bassoon with DLC, IC74, myosin V, Piccolo, and cytochrome *c* and of IC74 with DLC. Fig. S5 shows that Bsn9 pulls down DLC from brain extract and, when overexpressed, interferes with Bassoon transport in neurons. Video 1 shows cotransport of mRFP-Bassoon with DLC1-EGFP in neurons. Videos 2 and 3 show the mobility of particles marked with GFP-Bsn and GFP-BsnDBM in neurons. Online supplemental material is available at http://www.jcb.org/cgi/content/full/jcb.200807155/DC1.

We are grateful to H. Wickborn, J. Juhle, and B. Kracht for expert technical assistance, R. Frischknecht and M. Heine for helpful discussions and suggestions, T.A. Ryan for the EGFP-synapsin construct, and M. Sheng and R. Jahn for rabbit anti-DLC1/2 and synaptophysin antibodies, respectively.

This work has been supported by grants from the European Commission (SynScaff), the Land Saxony-Anhalt (LSA-N2), the European Union Structural Funds 2007–2013, and the Deutsche Forschungsgemeinschaft (SFB779/GRK1167) and a Max Planck Award from the Alexander von Humboldt Foundation/Max Planck Society to E.D. Gundelfinger. This work was also supported by grants from the German Federal Government (BMBF/01GA0505) to M.R. Kreutz, E.D. Gundelfinger, and N.E. Ziv and the National Institutes of Health (NS39471 and NS353862) to C.C. Garner. During part of the work, A. Fejtova was supported by a fellowship from the Swiss National Science Foundation.

Submitted: 28 July 2008
Accepted: 24 March 2009

References

Andrews-Zwilling, Y.S., H. Kawabe, K. Reim, F. Varoqueaux, and N. Brose. 2006. Binding to Rab3A-interacting molecule RIM regulates the presynaptic recruitment of Munc13-1 and ubMunc13-2. *J. Biol. Chem.* 281:19720–19731.

Barbar, E. 2008. Dynein light chain LC8 is a dimerization hub essential in diverse protein networks. *Biochemistry*. 47:503–508.

Bolte, S., and F.P. Cordelieres. 2006. A guided tour into subcellular colocalization analysis in light microscopy. *J. Microsc.* 224:213–232.

Bresler, T., M. Shapira, T. Boeckers, T. Dresbach, M. Futter, C.C. Garner, K. Rosenblum, E.D. Gundelfinger, and N.E. Ziv. 2004. Postsynaptic density assembly is fundamentally different from presynaptic active zone assembly. *J. Neurosci.* 24:1507–1520.

Burton, P.R., and J.L. Paige. 1981. Polarity of axoplasmic microtubules in the olfactory nerve of the frog. *Proc. Natl. Acad. Sci. USA*. 78:3269–3273.

Cai, Q., P.Y. Pan, and Z.H. Sheng. 2007. Syntabulin-kinesin-1 family member 5B-mediated axonal transport contributes to activity-dependent presynaptic assembly. *J. Neurosci.* 27:7284–7296.

Catimel, B., M. Nerrie, F.T. Lee, A.M. Scott, G. Ritter, S. Welt, L.J. Old, A.W. Burgess, and E.C. Nice. 1997. Kinetic analysis of the interaction between the monoclonal antibody A33 and its colonic epithelial antigen by the use of an optical biosensor. A comparison of immobilisation strategies. *J. Chromatogr. A*. 776:15–30.

Dick, O., I. Hack, W.D. Altrock, C.C. Garner, E.D. Gundelfinger, and J.H. Brandstatter. 2001. Localization of the presynaptic cytomatrix protein Piccolo at ribbon and conventional synapses in the rat retina: comparison with Bassoon. *J. Comp. Neurol.* 439:224–234.

Dillman, J.F. III, and K.K. Pfister. 1994. Differential phosphorylation in vivo of cytoplasmic dynein associated with anterogradely moving organelles. *J. Cell Biol.* 127:1671–1681.

Dresbach, T., A. Hempelmann, C. Spilker, S. tom Dieck, W.D. Altrock, W. Zuschratter, C.C. Garner, and E.D. Gundelfinger. 2003. Functional regions of the presynaptic cytomatrix protein bassoon: significance for synaptic targeting and cytomatrix anchoring. *Mol. Cell. Neurosci.* 23:279–291.

Dresbach, T., V. Torres, N. Wittenmayer, W.D. Altrock, P. Zamorano, W. Zuschratter, R. Nawrotzki, N.E. Ziv, C.C. Garner, and E.D. Gundelfinger. 2006. Assembly of active zone precursor vesicles: obligatory trafficking of presynaptic cytomatrix proteins Bassoon and Piccolo via a trans-Golgi compartment. *J. Biol. Chem.* 281:6038–6047.

Espindola, F.S., D.M. Suter, L.B. Partata, T. Cao, J.S. Wolenski, R.E. Cheney, S.M. King, and M.S. Mooseker. 2000. The light chain composition of chicken brain myosin-Va: calmodulin, myosin-II essential light chains, and 8-kDa dynein light chain/PIN. *Cell Motil. Cytoskeleton*. 47:269–281.

Fan, J., Q. Zhang, H. Tochio, M. Li, and M. Zhang. 2001. Structural basis of diverse sequence-dependent target recognition by the 8 kDa dynein light chain. *J. Mol. Biol.* 306:97–108.

Fejtova, A., and E.D. Gundelfinger. 2006. Molecular organization and assembly of the presynaptic active zone of neurotransmitter release. *Results Probl. Cell Differ.* 43:49–68.

Fenster, S.D., W.J. Chung, R. Zhai, C. Cases-Langhoff, B. Voss, A.M. Garner, U. Kaempf, S. Kindler, E.D. Gundelfinger, and C.C. Garner. 2000. Piccolo, a presynaptic zinc finger protein structurally related to bassoon. *Neuron*. 25:203–214.

Friedman, H.V., T. Bresler, C.C. Garner, and N.E. Ziv. 2000. Assembly of new individual excitatory synapses: time course and temporal order of synaptic molecule recruitment. *Neuron*. 27:57–69.

Frischknecht, R., A. Fejtova, M. Viesti, A. Stephan, and P. Sonderegger. 2008. Activity-induced synaptic capture and exocytosis of the neuronal serine protease neurotrypsin. *J. Neurosci.* 28:1568–1579.

Fuhrmann, J.C., S. Kins, P. Rostaing, O. El Far, J. Kirsch, M. Sheng, A. Triller, H. Betz, and M. Kneussel. 2002. Gephyrin interacts with Dynein light chains 1 and 2, components of motor protein complexes. *J. Neurosci.* 22:5393–5402.

Gindhart, J.G. Jr., C.J. Desai, S. Beushausen, K. Zinn, and L.S. Goldstein. 1998. Kinesin light chains are essential for axonal transport in *Drosophila*. *J. Cell Biol.* 141:443–454.

Goldstein, L.S. 2001. Kinesin molecular motors: transport pathways, receptors, and human disease. *Proc. Natl. Acad. Sci. USA*. 98:6999–7003.

Gross, S.P., M.A. Welte, S.M. Block, and E.F. Wieschaus. 2000. Dynein-mediated cargo transport in vivo. A switch controls travel distance. *J. Cell Biol.* 148:945–956.

Gross, S.P., M.A. Welte, S.M. Block, and E.F. Wieschaus. 2002. Coordination of opposite-polarity microtubule motors. *J. Cell Biol.* 156:715–724.

He, Y., F. Francis, K.A. Myers, W. Yu, M.M. Black, and P.W. Baas. 2005. Role of cytoplasmic dynein in the axonal transport of microtubules and neurofilaments. *J. Cell Biol.* 168:697–703.

Hirokawa, N., and R. Takemura. 2005. Molecular motors and mechanisms of directional transport in neurons. *Nat. Rev. Neurosci.* 6:201–214.

Jaffrey, S.R., and S.H. Snyder. 1996. PIN: an associated protein inhibitor of neuronal nitric oxide synthase. *Science*. 274:774–777.

Kanaji, S., J. Iwahashi, Y. Kida, M. Sakaguchi, and K. Mihara. 2000. Characterization of the signal that directs Tom20 to the mitochondrial outer membrane. *J. Cell Biol.* 151:277–288.

Krueger, S.R., A. Kolar, and R.M. Fitzsimonds. 2003. The presynaptic release apparatus is functional in the absence of dendritic contact and highly mobile within isolated axons. *Neuron*. 40:945–957.

Lai, M., F. Wang, J.G. Rohan, Y. Maeno-Hikichi, Y. Chen, Y. Zhou, G. Gao, W.A. Sather, and J.F. Zhang. 2005. A tctex1-Ca2+ channel complex for selective surface expression of Ca2+ channels in neurons. *Nat. Neurosci.* 8:435–442.

Lajoix, A.D., R. Gross, C. Aknin, S. Dietz, C. Granier, and D. Laune. 2004. Cellulose membrane supported peptide arrays for deciphering protein-protein interaction sites: the case of PIN, a protein with multiple natural partners. *Mol. Divers.* 8:281–290.

Leal-Ortiz, S., C.L. Waites, R. Terry-Lorenzo, P. Zamorano, E.D. Gundelfinger, and C.C. Garner. 2008. Piccolo modulation of Synapsin1a dynamics regulates synaptic vesicle exocytosis. *J. Cell Biol.* 181:831–846.

Lee, K.H., S. Lee, B. Kim, S. Chang, S.W. Kim, J.S. Paick, and K. Rhee. 2006. Dazl can bind to dynein motor complex and may play a role in transport of specific mRNAs. *EMBO J.* 25:4263–4270.

Liang, J., S.R. Jaffrey, W. Guo, S.H. Snyder, and J. Clardy. 1999. Structure of the PIN/LC8 dimer with a bound peptide. *Nat. Struct. Biol.* 6:735–740.

Lo, K.W., S. Naisbitt, J.S. Fan, M. Sheng, and M. Zhang. 2001. The 8-kDa dynein light chain binds to its targets via a conserved (K/R)XTQT motif. *J. Biol. Chem.* 276:14059–14066.

Maas, C., N. Tagnaouti, S. Loebrich, B. Behrend, C. Lappe-Siefke, and M. Kneussel. 2006. Neuronal cotransport of glycine receptor and the scaffold protein gephyrin. *J. Cell Biol.* 172:441–451.

Martin, M., S.J. Iyadurai, A. Gassman, J.G. Gindhart Jr., T.S. Hays, and W.M. Saxton. 1999. Cytoplasmic dynein, the dynactin complex, and kinesin are interdependent and essential for fast axonal transport. *Mol. Biol. Cell*. 10:3717–3728.

Miller, K.E., J. DeProto, N. Kaufmann, B.N. Patel, A. Duckworth, and D. Van Vactor. 2005. Direct observation demonstrates that Liprin-alpha is required for trafficking of synaptic vesicles. *Curr. Biol.* 15:684–689.

Naisbitt, S., J. Valtschanoff, D.W. Allison, C. Sala, E. Kim, A.M. Craig, R.J. Weinberg, and M. Sheng. 2000. Interaction of the postsynaptic density-95/guanylate kinase domain-associated protein complex with a light chain of myosin-V and dynein. *J. Neurosci.* 20:4524–4534.

Navarro, C., H. Puthalakath, J.M. Adams, A. Strasser, and R. Lehmann. 2004. Egalitarian binds dynein light chain to establish oocyte polarity and maintain oocyte fate. *Nat. Cell Biol.* 6:427–435.

Ohtsuka, T., E. Takao-Rikitsu, E. Inoue, M. Inoue, M. Takeuchi, K. Matsubara, M. Deguchi-Tawarada, K. Satoh, K. Morimoto, H. Nakanishi, and Y. Takai. 2002. Cast: a novel protein of the cytomatrix at the active zone of synapses that forms a ternary complex with RIM1 and munc13-1. *J. Cell Biol.* 158:577–590.

Okada, Y., H. Yamazaki, Y. Sekine-Aizawa, and N. Hirokawa. 1995. The neuron-specific kinesin superfamily protein KIF1A is a unique monomeric motor for anterograde axonal transport of synaptic vesicle precursors. *Cell*. 81:769–780.

Pfister, K.K., E.M. Fisher, I.R. Gibbons, T.S. Hays, E.L. Holzbaur, J.R. McIntosh, M.E. Porter, T.A. Schroer, K.T. Vaughan, G.B. Witman, et al. 2005. Cytoplasmic dynein nomenclature. *J. Cell Biol.* 171:411–413.

Puthalakath, H., A. Villunger, L.A. O'Reilly, J.G. Beaumont, L. Coultas, R.E. Cheney, D.C. Huang, and A. Strasser. 2001. Bmf: a proapoptotic BH3-only protein regulated by interaction with the myosin V actin motor complex, activated by anoikis. *Science*. 293:1829–1832.

Sabo, S.L., R.A. Gomes, and A.K. McAllister. 2006. Formation of presynaptic terminals at predefined sites along axons. *J. Neurosci.* 26:10813–10825.

Schikorski, T., and C.F. Stevens. 1999. Quantitative fine-structural analysis of olfactory cortical synapses. *Proc. Natl. Acad. Sci. USA*. 96:4107–4112.

Schnorrer, F., K. Bohmann, and C. Nusslein-Volhard. 2000. The molecular motor dynein is involved in targeting swallow and bicoid RNA to the anterior pole of *Drosophila* oocytes. *Nat. Cell Biol.* 2:185–190.

Schroer, T.A., S.T. Brady, and R.B. Kelly. 1985. Fast axonal transport of foreign synaptic vesicles in squid axoplasm. *J. Cell Biol.* 101:568–572.

Shapira, M., R.G. Zhai, T. Dresbach, T. Bresler, V.I. Torres, E.D. Gundelfinger, N.E. Ziv, and C.C. Garner. 2003. Unitary assembly of presynaptic active zones from Piccolo-Bassoon transport vesicles. *Neuron*. 38:237–252.

Shin, H., M. Wyszynski, K.H. Huh, J.G. Valtschanoff, J.R. Lee, J. Ko, M. Streuli, R.J. Weinberg, M. Sheng, and E. Kim. 2003. Association of the kinesin motor KIF1A with the multimodular protein liprin-alpha. *J. Biol. Chem.* 278:11393–11401.

Su, Q., Q. Cai, C. Gerwin, C.L. Smith, and Z.H. Sheng. 2004. Syntabulin is a microtubule-associated protein implicated in syntaxin transport in neurons. *Nat. Cell Biol.* 6:941–953.

Tao-Cheng, J.H. 2007. Ultrastructural localization of active zone and synaptic vesicle proteins in a preassembled multi-vesicle transport aggregate. *Neuroscience*. 150:575–584.

tom Dieck, S., L. Sanmarti-Vila, K. Langnaese, K. Richter, S. Kindler, A. Soyke, H. Wex, K.H. Smalla, U. Kampf, J.T. Franzer, et al. 1998. Bassoon, a novel zinc-finger CAG/glutamine-repeat protein selectively localized at the active zone of presynaptic nerve terminals. *J. Cell Biol.* 142:499–509.

tom Dieck, S., W.D. Altrock, M.M. Kessels, B. Qualmann, H. Regus, D. Brauner, A. Fejtova, O. Bracko, E.D. Gundelfinger, and J.H. Brandstatter. 2005. Molecular dissection of the photoreceptor ribbon synapse: physical interaction of Bassoon and RIBEYE is essential for the assembly of the ribbon complex. *J. Cell Biol.* 168:825–836.

Tsuriel, S., R. Geva, P. Zamorano, T. Dresbach, T. Boeckers, E.D. Gundelfinger, C.C. Garner, and N.E. Ziv. 2006. Local sharing as a predominant determinant of synaptic matrix molecular dynamics. *PLoS Biol.* 4:e271.

Tsuriel, S., A. Fisher, N. Wittenmayer, T. Dresbach, C.C. Garner, and N.E. Ziv. 2009. Exchange and redistribution dynamics of the cytoskeleton of the active zone molecule bassoon. *J. Neurosci.* 29:351–358.

Vadlamudi, R.K., R. Bagheri-Yarmand, Z. Yang, S. Balasenthil, D. Nguyen, A.A. Sahin, P. den Hollander, and R. Kumar. 2004. Dynein light chain 1, a p21-activated kinase 1-interacting substrate, promotes cancerous phenotypes. *Cancer Cell*. 5:575–585.

Vale, R.D. 2003. The molecular motor toolbox for intracellular transport. *Cell*. 112:467–480.

Vallee, R.B., J.C. Williams, D. Varma, and L.E. Barnhart. 2004. Dynein: An ancient motor protein involved in multiple modes of transport. *J. Neurobiol.* 58:189–200.

Wang, X., M. Kibschull, M.M. Laue, B. Lichte, E. Petrasch-Parwez, and M.W. Kilimann. 1999. Aczonin, a 550-kD putative scaffolding protein of presynaptic active zones, shares homology regions with Rim and Bassoon and binds profilin. *J. Cell Biol.* 147:151–162.

Welte, M.A. 2004. Bidirectional transport along microtubules. *Curr. Biol.* 14:R525–R537.

Williams, J.C., P.L. Roulhac, A.G. Roy, R.B. Vallee, M.C. Fitzgerald, and W.A. Hendrickson. 2007. Structural and thermodynamic characterization of a cytoplasmic dynein light chain-intermediate chain complex. *Proc. Natl. Acad. Sci. USA*. 104:10028–10033.

Zhai, R., G. Olias, W.J. Chung, R.A. Lester, S. tom Dieck, K. Langnaese, M.R. Kreutz, S. Kindler, E.D. Gundelfinger, and C.C. Garner. 2000. Temporal appearance of the presynaptic cytomatrix protein bassoon during synaptogenesis. *Mol. Cell. Neurosci.* 15:417–428.

Zhai, R.G., H. Vardinon-Friedman, C. Cases-Langhoff, B. Becker, E.D. Gundelfinger, N.E. Ziv, and C.C. Garner. 2001. Assembling the presynaptic active zone: a characterization of an active one precursor vesicle. *Neuron*. 29:131–143.